frontiers in Energy Research

REVIEW
published: 03 September 2020
doi: 10.3389/fenrg.2020.571440

Manufacturing Strategies for Solid Electrolyte in Batteries

*Annan Chen[1,2†], Conghang Qu[3†], Yusheng Shi[2] and Feifei Shi[1]**

[1] Department of Energy and Mineral Engineering, The Pennsylvania State University, University Park, PA, United States, [2] State Key Laboratory of Materials Processing and Die and Mould Technology, School of Materials Science and Engineering, Huazhong University of Science and Technology, Wuhan, China, [3] Department of Materials Science and Engineering, The Pennsylvania State University, University Park, PA, United States

Throughout the development of battery technologies in recent years, the solid-state electrolyte (SSE) has demonstrated outstanding advantages in tackling the safety shortcomings of traditional batteries while meeting high demands on electrochemical performances. The traditional manufacturing strategies can achieve the fabrication of batteries with simple forms (coin, cylindrical, and pouch), but encounter limitations in preparing complex-shaped or micro/nanoscaled batteries especially for inorganic solid electrolytes (ISEs). The advancement in novel manufacturing techniques like 3D printing has enabled the assembly of different solid electrolytes (polymeric, inorganic, and composites) in a more complex geometric configuration. However, there is a huge gap between the capabilities of the current 3D printing techniques and the requirements for battery production. In this review, we compare the traditional manufacturing to several novel 3D printing techniques, highlighting the potential of 3D printing in the SSE manufacturing. The latest SSE manufacturing progress in the group of direct-writing (DW) based or lithography-based printing technologies are summarized separately from the perspectives of feedstock selection, build envelope, printing resolution, and application (nano-scaled, flexible, and large-scale battery grids). Throughout the discussion, some challenges associated with manufacturing SSEs via 3D printing such as air/moisture sensitivity of samples, printing resolution, scale-up capability, and long-term sintering for ISEs have been put forward. This review aims to bridge the gap between 3D printing techniques and battery requirements by analyzing the existing limitation in SSE manufacturing and point out future needs.

Keywords: manufacture, 3D printing, direct-write, stereolithography, solid electrolyte, battery

OPEN ACCESS

Edited by:
Zhengcheng (John) Zhang, Argonne National Laboratory (DOE), United States

Reviewed by:
Huan Pang, Yangzhou University, China
Zonghai Chen, Argonne National Laboratory (DOE), United States

****Correspondence:***
Feifei Shi
feifeishi@psu.edu

† These authors have contributed equally to this work

Specialty section:
This article was submitted to Electrochemical Energy Conversion and Storage, a section of the journal Frontiers in Energy Research

Received: *10 June 2020*
Accepted: *14 August 2020*
Published: *03 September 2020*

Citation:
Chen A, Qu C, Shi Y and Shi F (2020) Manufacturing Strategies for Solid Electrolyte in Batteries. Front. Energy Res. 8:571440. doi: 10.3389/fenrg.2020.571440

Abbreviations: 2D, two-dimensional; AJP, aerosol jet printing; CLIP, continuous liquid interface production; CSE, composite solid electrolytes; DIW, direct ink writing; DLP, digital light processing; DMD, digital micromirror device; DW, direct writing; FDM, fused deposition modeling; GO, graphene oxide; IJP, inkjet printing; ISE, inorganic solid electrolyte; LAGP, $Li_{1.4}Al_{0.4}Ge_{1.6}(PO_4)_3$; LFP, $LiFePO_4$; LIB, li-ion batteries; LLZ, $Li_7La_3Zr_2O_{12}$; LTO, $Li_4Ti_5O_{12}$; PμSL, projection micro stereolithography; PLA, polylactic acid; SL, stereolithography; SOFC, solid oxide fuel cell; SPE, solid polymer electrolyte; SSE, solid-state electrolyte; TPP, two-photon polymerization; UV, ultraviolet; YSZ, yttria-stabilized zirconia.

INTRODUCTION

The popularization of commercial batteries is one of the highlights of modern civilization. In the past few decades, society has witnessed the invention of self-powered medical implant devices, wireless electronics, electric vehicles, and many other applications that are powered by batteries with different shapes and sizes. Traditional batteries using organic liquid electrolytes have demonstrated the benefits of high ionic conductivity and excellent wettability with electrodes (Zhang, 2007; He et al., 2019), but suffer from potential safety issues such as high flammability, poor thermal stability, and liquid leakage (Strauss et al., 2020; Yin et al., 2020; Yuan and Liu, 2020). To tackle the inherent safety shortcomings of traditional batteries while meeting high demands on electrochemical performances, batteries using the solid-state electrolyte (SSE) has demonstrated a promising choice to be the better alternatives.

Generally, the SSE can be classified into solid polymer electrolytes (SPEs), inorganic solid electrolytes (ISEs), and composite solid electrolytes (CSEs). SPEs are constituted of a high molecular-weight polymer matrix and a dissolved lithium salt, ISEs are composed of all inorganic materials such as ceramics and glass, and CSEs consisting of both solid polymer and the inorganics (Zhang H. et al., 2017; Chen W. et al., 2018; Chen Y. et al., 2020). As one key component for the practical application of solid-state batteries, SSEs have demonstrated numerous advantages over the organic liquid electrolyte: (i) the characteristics of non-flammability, high-temperature stability, and non-volatilization to eliminate the combustion or explosion of organic liquid electrolytes (Fergus, 2010; Takada, 2013; Sun et al., 2020), (ii) a wide electrochemical window to enable better compatibility with a higher-potential cathode, which greatly improves the energy density (Judez et al., 2017; Wang et al., 2018), (iii) an improved mechanical rigidity (especially for ISEs) to suppress dendrite growth from cycled metallic anodes (Goodenough and Singh, 2015; Kim J.G. et al., 2015), and (iv) a tunable elastic modulus (especially for SPEs and CSEs) allowing for a higher degree of processability and flexibility (Yue et al., 2016; Lau et al., 2018; Schnell et al., 2018; Zhou et al., 2018). However, several challenges should be further investigated and addressed: (i) the low ionic conductivity ($<10^{-5}$ S cm^{-1} for SPEs and $<10^{-3}$ S cm^{-1} for ISEs) compared with the liquid electrolyte ($>10^{-3}$ S cm^{-1}) that leads to a low power rate, and (ii) the difficulty in manufacturing miniature/large ISEs with high brittleness. Combined with novel materials design, the development of advanced manufacturing strategies will provide solutions to the above issues.

The growth in battery technologies has shown an exponential trend since the 1800s, and we have witnessed the motivation behind battery development to gradually transition from enhancing electrochemical cell performances to meeting configurational demands of complex applications. **Figure 1** shows several notable milestones in the evolution of battery manufacturing. As the earliest documented battery invention, the voltaic pile consisted of the stacking of copper, zinc, and saltwater-soaked cloth in a cylindrical fashion to store electrochemical energy (Abetti, 1952; Warner, 2015). Nearly six decades later, Gaston Plante (Kurzweil, 2010) submerged packs of parallel lead/lead oxide plates in sulfuric acid and created the first rechargeable battery. Both voltaic pile and lead-acid batteries relied on the stacking of metal plates to increase the cell voltage (Warner, 2015). As the evolution continues, nickel-cadmium battery used a cylindrical cell filled with compacted metal-sheet electrodes rolled into a coil with increased surface area to reduce battery resistance. This cylindrical design was adopted by the later commercial alkaline battery with electrode materials filled in the inner and outer layers (Furukawa et al., 1984). In 1971, the invention of lithium-iodine batteries made a significant contribution to the medical device industry. This battery cell used a metal pouch with rounded edges to prevent penetration issues that sharp corners might cause when implanted in the human body as part of the cardiac pacemakers (Greatbatch and Holmes, 1991; Ruetschi et al., 1995).

Since the commercialization of Li-ion batteries (LIBs) by Sony Co. in 1991 (Yoshio et al., 2009), many traditional and novel form factors have been applied in LIBs to enable the development of better products in terms of aesthetics and functionality. Li-ion prismatic cells utilized the compacted and rolled electrodes previously seen in nickel-cadmium batteries and packed them in containers with shapes visually resembled by a flat chocolate bar (Cousseau et al., 2006). Li-ion pouch cells achieved a high 90–95% packing efficiency by welding the conductive tabs with electrode foils and hermetically sealed all materials within the pouch (Buchmann, 2001). The invention of both Li-ion prismatic and pouch cells is part of the effort to achieve thinner and lighter electronics. With the progress in technological maturity and complexity in recent years, new manufacturing strategies can be applied to batteries at different scales that are suitable for various applications. For example, nano-scaled batteries used as the power source in biomedical applications (Johannessen et al., 2006; Ruzmetov et al., 2012), flexible batteries for foldable/wearable electronics (Dudney, 2008; Leijonmarck et al., 2013; Deng et al., 2017), and potentially large-scale battery grids for renewable energy storage (Diouf and Pode, 2015). However, the traditional battery manufacturing strategies such as dry-pressing, casting, spin coating, and roll to roll are unsatisfactory in preparing complex-shaped or micro/nanoscale batteries especially for ISEs (Manthiram et al., 2017; Schnell et al., 2018; Dirican et al., 2019). Therefore, there is an urge to exploit a novel manufacturing strategy to address the above issues.

The emergence of 3D printing technique offered a unique manufacturing method that has the feasibility to build parts with high complexity and fine features (Chen Z. et al., 2019; Santoliquido et al., 2019). Although using the 3D printing technique could be a promising alternative option in SSE manufacturing, the original purpose for the development of 3D printing was not targeted to produce batteries. As a result, there is a huge gap between the capabilities of the current 3D printing techniques and the requirements for battery production. This review aims to bridge the gap by analyzing the existing limitation in SSE manufacturing and point out future needs. Through a comprehensive overview of traditional and novel SSE manufacturing strategies, we set to provide guidance and enlightenment toward potential breakthroughs

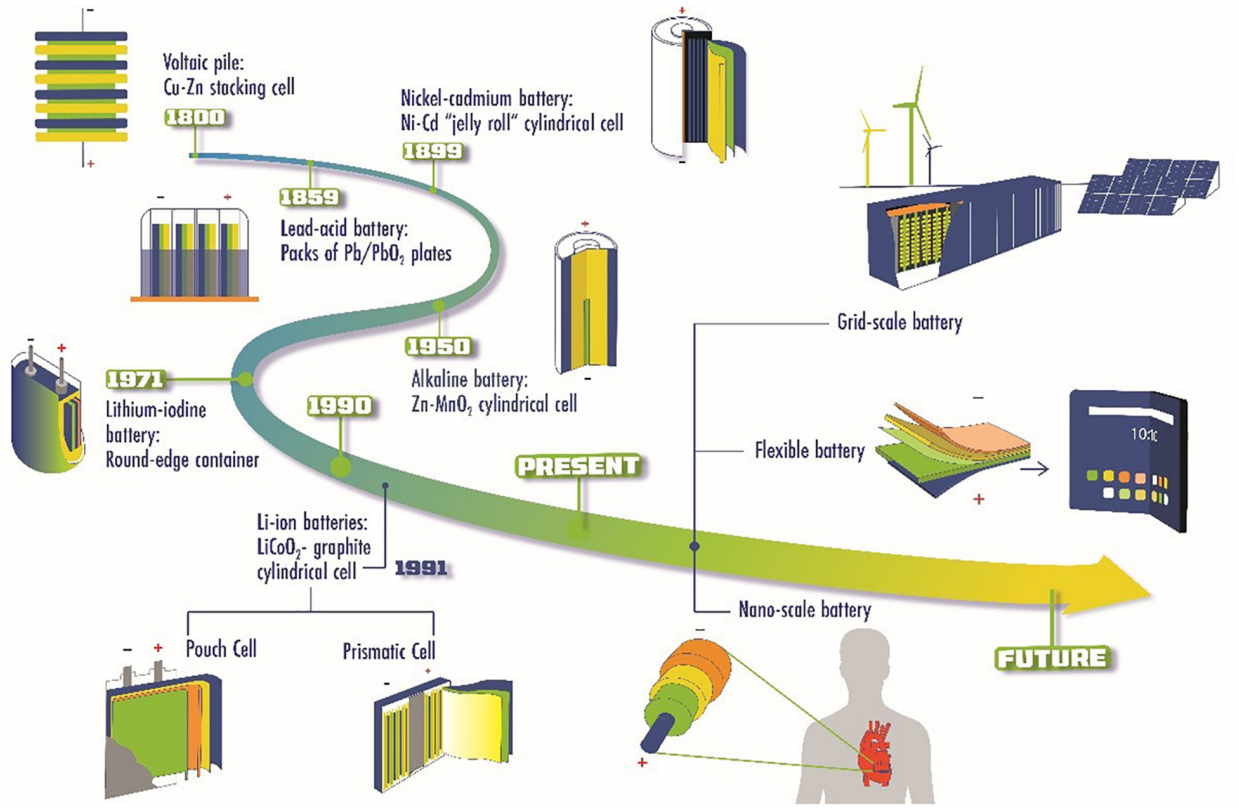

FIGURE 1 | Evolution of battery manufacturing.

in manufacturing techniques for both laboratory research and industrial production.

TRADITIONAL MANUFACTURING STRATEGIES

Solid Polymer/Composite Electrolytes

Solid polymer electrolytes (SPEs) have been extensively studied for foldable and stretchable batteries (Commarieu et al., 2018; Liang et al., 2018; Chen Y. et al., 2020) due to several advantages such as high flexibility, easy processability, and good wettability. Three different routes could be used to manufacture SPEs: powder-based processing, wet chemical processing, and high-viscosity processing. For powder-based processing, a dry milling process at a high speed is first used to prepare well-mixed fine powders, and then SPEs can be produced by dry-pressing (Li et al., 2018), hot/cold isostatic pressing (Appetecchi et al., 2001), or deposition process (Hafner et al., 2019). The advantages of powder-based processing are simple operation, low equipment requirements, and possible densification-step avoidance (Nguyen et al., 2019). However, this process is time-intensive, energy-consuming, and difficult to scale up. For wet chemical processing, raw particles are first dispersed with a solvent to obtain a suspension with a target viscosity, and then SPEs are formed by solution casting (Sun et al., 2019), electrophoretic deposition (Blanga et al., 2015), or coating process (Park et al., 2006). The advantages of wet chemical processing are good wettability and high throughput (Liu et al., 2017). Disadvantages, however, are the necessity of solvent removal. For high-viscosity processing, a highly viscous solvent-free paste consisting of polymers is first prepared at elevated temperatures, and then an extrusion process is applied to generate SPEs with the desired form factor (Li W. et al., 2017), which is assisted with ultraviolet (UV) irradiation for interlinking polymer chains in some cases. The advantages of this process are the solvent-free processing, and the formation of low porosity and flexible membranes (Wang et al., 2005). Limited throughput during extrusion process and high defect rate in uneven deposited polymer films can be the disadvantages. The main challenges of SPEs are the low ionic conductivity of 10^{-8}∼10^{-5} S cm^{-1} at ambient temperature (Liang et al., 2018), and high interfacial resistance due to polymer insulating Li^{+} (Wan et al., 2019).

The CSEs consisting of polymer and inorganic portions are developed to achieve satisfactory comprehensive properties and exceptional synergistic effects compared to the single-component electrolyte. Due to the presence of polymer, the manufacturing strategies of the CSEs are similar to that of SPEs, which have been reported in the previous reviews (Commarieu et al., 2018; Liu et al., 2018; Tan et al., 2018; Li et al., 2020). One of the most popular technologies to prepare CSEs is electrospinning, which produces interlaced and highly porous nanofibers with a large

surface-to-volume ratio and improved mechanical strength due to the entanglement and reinforcing effects (Cavaliere et al., 2011; Wootthikanokkhan et al., 2015; Carli et al., 2019). A common issue to be noted in CSE manufacturing is the limited mass loading of inorganic materials, which are easy to agglomerate and thus deteriorating the ionic conductivity and mechanical strength of batteries. Overall, SPEs and CSEs have a high degree of processability due to the high flexibility of polymer materials.

Inorganic Solid Electrolytes

Inorganic solid electrolytes can be divided into groups of crystalline, glass, and glass-ceramic electrolytes. The majority of crystalline electrolytes are ceramics such as NASICON-type, Perovskite-type, and Garnet-type, which are stable in ambient air that can simplify cell fabrication and improve safety. The ceramic electrolyte is typically prepared by the dry-pressing method with subsequent high-temperature sintering (Li C. et al., 2019). To perform dry-pressing to obtain a dense ceramic electrolyte, the fine-milled powders need to premix with ∼5 wt% polyvinyl alcohol, which easily generates micro-/macropore defects after binder remover treatment. Besides, the pressure on the powder at different positions along the axial direction is unequal, resulting in uneven density and composition of the dry-pressed sample (Suvacı and Messing, 2001; Tanaka et al., 2006; Schiavo et al., 2018). Alternatively, a colloidal process can be selected to prepare ceramic electrolytes with high relative density and good composition uniformity (Lewis, 2004; Franks et al., 2017). In colloidal forming, the preparation of suspensions with a high solid loading (>50 vol%) and low viscosity [<1 Pa·s at the shear rate of 100 s^{-1} (Tallon and Franks, 2011; Chen A.N. et al., 2020)] is the key factor for non-porous casting and dense ceramic preparation. It should be noted that ceramic electrolytes typically require care in selecting solvents as they may cause unwanted component diffusion or reaction (Li B. et al., 2017; Lim et al., 2018; Hitz et al., 2019). Another part of the crystalline electrolyte is thio-LISICON (Li_2S-P_2S_5 system), which could achieve a high ion conductivity of 10^{-3}∼10^{-2} S cm^{-1} due to the more polarizable electron cloud of sulfur (Zhang et al., 2019; Shan et al., 2020). The manufacturing process of thio-LISICON electrolyte is similar to ceramic electrolytes, while a controlled inert atmosphere is typically required due to its air-sensitivity (Manthiram et al., 2017). Besides, the crystalline electrolyte can also be manufactured by the thin-film processing such as pulsed laser deposition (Fujimoto et al., 2015), chemical vapor deposition (Gelfond et al., 2009), sputter deposition (Lethien et al., 2011), sol-gel deposition (Jung et al., 2001), etc.

The glassy electrolytes have attracted great attention due to their several advantages over the crystalline materials: isotropic ionic conduction, no grain boundary resistance, ease to be fabricated into a film, ease of composition modifications, etc. In general, there are four main processing methods to form glassy electrolytes: melt-quenching, mechanical milling, sol-gel synthesis, and wet chemical reaction. The melt-quenching method involves the initial preheating/melting of pristine materials to generally above 900°C and the subsequent pressing/annealing (Pradel et al., 1985). It is the most commonly used method to produce glassy and glass-ceramic electrolytes. Due to the strong propensity toward the crystallization of some glass compositions, a twin-roller quenching apparatus is used to achieve a high cooling rate by reducing the volume of the melted glass (Pradel et al., 1985; Minami et al., 2006). As a drawback, the melt-quenching method does involve high temperatures and a rather complicated setup that could be potentially hazardous. Benefited from the simplicity of manufacturing procedures and the ability to enhance size reduction/uniformity at the ambient temperature and pressure, the mechanical milling method can be easily applied to produce large amounts of well-mixed fine powders at low cost. However, the amorphization process during milling does have a strong time dependence and it could take up to 20 h to observe the amorphous halo on X-ray diffraction patterns (Morimoto et al., 1999; Hayashi et al., 2002). The sol-gel synthesis method to manufacture glassy electrolytes involves the process of controlled hydrolysis, polycondensation, gelation, and dehydration (Hench and West, 1990). Depending on the glass composition, various metal alkoxides or inorganics are used as precursors to mix with appropriate solvent for the hydrolyzation step. The following condensation reaction then forms the bonding and linkage for the backbone of the glass network (Hench and West, 1990). Due to a liquid-state reaction and mixing, the sol-gel synthesis can achieve high homogeneity at relatively low temperatures (Hench and West, 1990; Venkatasubramanian et al., 1991; Dunn et al., 1994). Similar to procedures of sol-gel synthesis, the wet chemical reaction method can obtain the desired composition via molecule/bonding rearrangement during the liquid-state reaction. Organic compounds are generally used as the solvent to dissolve starting chemicals (Teragawa et al., 2014; Phuc et al., 2016; Choi et al., 2017).

Glass-ceramic electrolytes comprise a class of materials with a mixture of both amorphous and microcrystalline microstructure that is commonly obtained through controlled nucleation and crystallization treatment of the corresponding glass material at a temperature above the glass transition temperature (Varshneya and Mauro, 2019). Similar to the common manufacturing techniques of glassy electrolytes, many previous literatures have reported the glass-ceramic electrolytes obtained by melt-quenching or mechanical milling following by an annealing step (Hayashi et al., 2003; Trevey et al., 2009; Tatsumisago and Hayashi, 2012). However, the annealing temperature and time could affect the structural arrangements of the crystalline phases and impact the ionic conductivity (Xie et al., 2009). The use of sol-gel synthesis and the wet chemical reaction methods in producing glass-ceramics ISEs have also been reported in several recent works (Kotobuki et al., 2013; Teragawa et al., 2014; Li et al., 2015; Ma et al., 2016; Phuc et al., 2016).

Although ISEs offer numerous benefits in solid-state battery technology, their brittle nature brings numerous processing and integration challenges. After ISEs fabrication, post-treatments such as grinding or cutting are typically required to attain the desired forms to combine with electrode layers. However, many ISE materials inevitably face the dilemma of undergoing chemical cross-contamination or structural damage during post-treatments. For example, ceramic electrolytes could fracture during cutting, and glass/glass-ceramics electrolytes

could have side reactions associated with water or elevated temperature during grinding/polishing. Therefore, the post-treatments could significantly increase manufacturing costs and extends the production cycle. A summary of the traditional SSE manufacturing techniques is provided via the schematics in **Figure 2**, where those common techniques presented similar limitations in achieving the complex form factors required by future battery applications. Under this circumstance, the research on 3D printing SSEs has drawn increasing attention due to its capability of achieving one-step manufacturing of SSEs with desired form factors. Bypassing many additional steps required by the traditional methods, the fully integrated manufacturing of an entire solid-state battery could also be achieved through 3D printing in the future. In the following, this review will discuss the existing 3D printing strategies for SSEs, and then emphasize the prospects and feasibility to enhance the performance of 3D-printed SSEs.

3D PRINTING TECHNOLOGIES

Additive Manufacturing, i.e., 3D printing, refers to an advanced fabrication technique that built three-dimensional objects in a layer-by-layer way based on computer-aid-design (CAD) files (Chen A.N. et al., 2017; Mao et al., 2017). Compared with the traditional method, the 3D printing technique has demonstrated unique advantages in the rapid prototyping of highly complex and precise structures. This advantage can significantly simplify the fabrication procedure and reduce material waste to save the production cost (Chen A.N. et al., 2018; Li M. et al., 2019). Besides, 3D printing is capable of alleviating inherent restrictions of form factor in batteries and transform battery manufacturing from simple two-dimensional to complex three-dimensional (Pang et al., 2019; Cheng et al., 2020; Yang et al., 2020). Given the above advantages, a couple of 3D printing techniques have been applied for SSE manufacturing. These SSE 3D printing techniques can be divided into the following two categories: the direct-write (DW)-based printing [such as direct ink writing (DIW), inkjet printing (IJP), aerosol jet printing (AJP), and fused deposition modeling (FDM)], and the lithography-based printing [such as stereolithography (SL), and digital light processing (DLP)]. The following will discuss the latest research progress of SSE 3D printing strategies, from the aspects of feedstock selection, build envelope, and printing resolution.

DW-Based 3D Printing of Solid-State Electrolytes

Direct Ink Writing

Direct ink writing (DIW) is the most widely used 3D printing technique for SSE manufacturing due to its low cost, easy operation, and broad feedstock selection (metals, polymers, and ceramics) (Ambrosi and Pumera, 2016; Du et al., 2017). A schematic of the DIW process is shown in **Figure 3A**. During the printing process, the gel-based viscoelastic inks are directly extruded from a nozzle head in the form of a continuous filament. By moving up the nozzle, the designed 3D objects can be created through a consecutive layer-by-layer deposition. After printing, the ink materials are rapidly solidified under the effects of solvent evaporation, gelation, temperature- or solvent-induced phase changes (Naficy et al., 2014). Typically, the printing resolution of DIW printed objects is determined by the nozzle diameter that is tens to hundreds of micrometers. To print SSEs with a high resolution (10–100 μm), the high performing ink formulation is a crucial factor. The printing ink must be modulated to acquire a good shear-thinning behavior allowing the smooth flow of inks through the nozzle, and a sufficiently high yield stress and storage modulus are required to enable the shape retention of extruded filaments (Chang et al., 2019).

In 2010, the first DIW printed ionic liquid gel SSE was reported by Ho et al. (2010). As shown in **Figure 3A**, the SSE was sandwiched between electrodes in Zn-MnO_2 micro-battery. The printed cell exhibited a storage capacity of 0.98 mAh cm^{-2} and an energy density of 1.2 mWh cm^{-2} over more than 70 cycles. Fu et al. (2016) printed polymer composite electrolyte inks with controllable viscosity for $Li_4Ti_5O_{12}$-graphene oxide (GO) interdigitated battery (**Figure 3B**). Noting that the GO flakes were controlled to align along the extruding direction in the deposited electrodes, which could improve the electrical conductivity, and provide sufficient surface area to host the electrolyte. CSEs were made for flexible LIBs by DIW (**Figures 3C,D**; Blake et al., 2017; Cheng et al., 2018). Compared with the commercial polyolefin separator, the printed CSEs demonstrated comparable high rate electrochemical performance, better thermal stability, electrolyte wettability, and cyclability (Blake et al., 2017). Mcowen et al. (2018) prepared $Li_7La_3Zr_2O_{12}$ (LLZ) ceramic electrolyte with different micrometer-scale features for Li metal battery (**Figure 3E**). These electrolyte structures had proven to bring batteries with good mechanical properties, lower full cell resistance, and improved energy and power density. Similar DIW work has also been reported in other literatures (Braam et al., 2012; Wei et al., 2018; Ma and Devin Mackenzie, 2019). The main advantages of DIW lie in its broad feedstock selection and wide range of build envelope (100 μm–10 cm). The use of concentrated viscoelastic pastes allows for building 3D structures without the need for supports (such as powder bed, liquid vat, or printed manual supports) (Chen Z. et al., 2019), which can simplify the printing process, omit the surface treatment process, and maximize feedstock utilization. DIW is well investigated to the manufacturing of tailor porous structures possessing periodic characteristics, with little or no resolution required. However, the preparation of gel-based viscoelastic pastes for DIW is challenging. Besides, the DIW printed features are limited to the woodpile structures owing to the extruded filament shapes, showing difficulties in fabricating dense structures.

Ink-Jet Printing

Ink-jet printing (IJP) is a non-contact droplet-based material deposition technique that can directly eject ink microdroplets through nozzles on different types of substrates to create two-dimensional (2D) patterns (Dobrozhan et al., 2020). A schematic of the IJP process is shown in **Figure 4A**. As a promising method, the IJP has been explored to print multiple materials including metal, polymers, so-gel, and protein materials, etc. (Fritzler and Prinz, 2017). Typically, the ink for the IJP must be

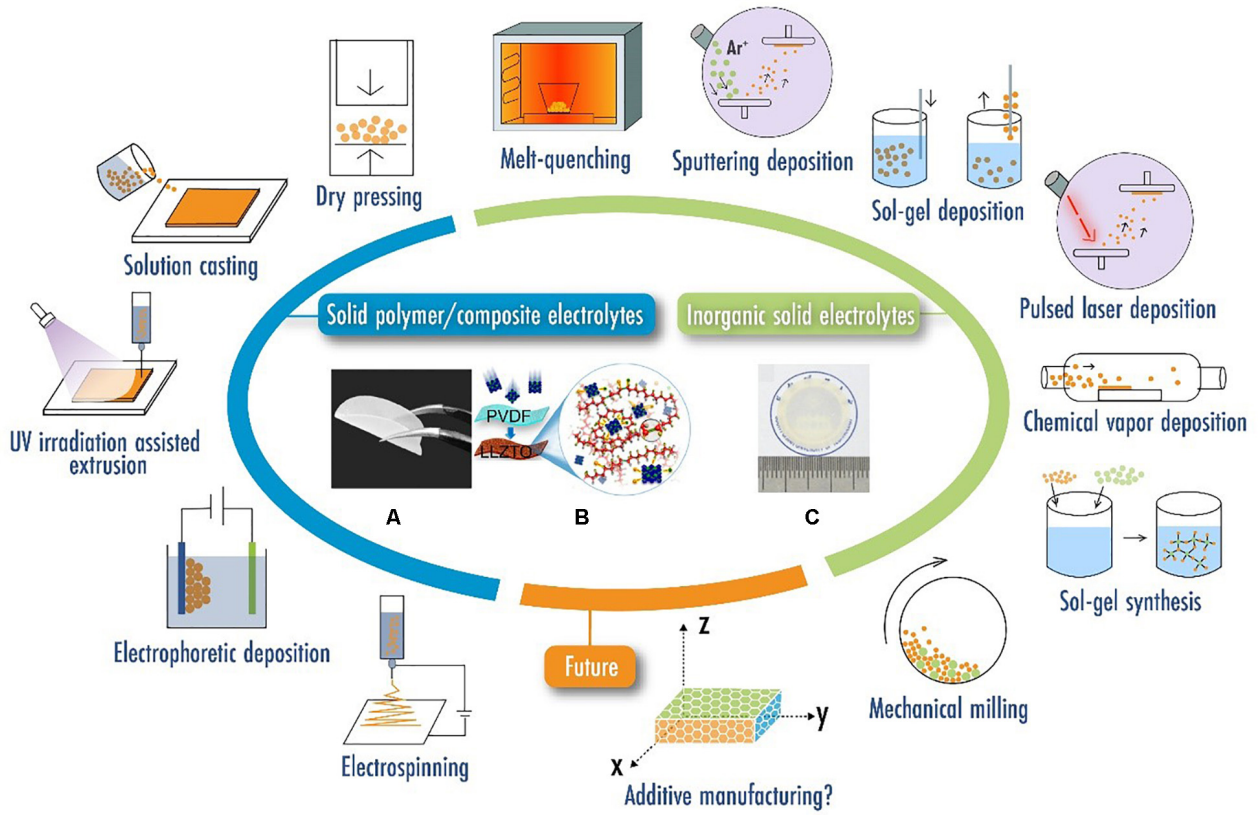

FIGURE 2 | Schematics of traditional manufacturing strategies with **(A)** Optical image of a polyethylene oxide (PEO) based solid polymer electrolyte. Reproduced from Chen C. et al. (2019) under the Creative Commons Attribution license. **(B)** Schematic of a solid composite electrolyte combining $Li_{6.75}La_3Zr_{1.75}Ta_{0.25}O_{12}$ (LLZTO) and polyvinylidene fluoride (PVDF). Reproduced from Zhang X. et al. (2017) with permission from John Wiley & Sons-Books. **(C)** Optical image of a $Li_{0.34}La_{0.56}TiO_3$ (LLTO) ceramic electrolyte film. Reproduced from Jiang et al. (2020) with permission from John Wiley & Sons-Books.

in a diluted liquid form with a sufficiently low dynamic viscosity and surface tension. A quantitative characterization based on the ink's physical properties was proposed by Derby (2010) to evaluate whether the ink can be described as the "printability" for IJP: $Z = 1/Oh = (\gamma\rho\alpha)^{1/2}/\eta$, where Z is the reciprocal of a dimensionless number, Oh is the Ohnesorge number, α is a characteristic length representing the nozzle radius, and ρ, η, and γ are the density, dynamic viscosity, and surface tension for the ink, respectively. In the case of $1 < Z < 10$, the ink is expected to produce stable droplets to enable the IJP process.

The application of IJP to printing SSEs was first described in the literature by Delannoy et al. (2015). The authors deposited silica-based ionogel inks directly onto porous composite electrodes to form SSE for LIBs (**Figures 4A–D**). The ionogel SSE showed high ionic conductivity, good thermal resistance, and excellent compatibility with porous electrodes that enabled the fabrication of micro-LIBs with high surface capacity and good electrochemical cycling performance. The full cell using IJP-printed ionogel SSE with $LiFePO_4$ and $Li_4Ti_5O_{12}$ porous composite electrodes exhibited a surface capacity of 300 mAh cm^{-2} for more than 100 cycles, which was more competitive than that of microdevices obtained by the expensive physical vapor deposition process. In the IJP technique, the diameter of the nozzle is typically less than 5 μm, which is smaller compared with that of DIW (tens to hundreds of micrometers). In this case, the IJP enables the fabrication of designed structures with a higher resolution (5–20 μm), which have promoted the application of IJP in the fields of microelectronics and energy devices. However, the IJP-printed objects are mostly limited to 2D space with a building envelope of 50 μm–10 mm, and not adaptable for depositing thick patterns owing to the very small volume of the feedstock inks. Besides, the IJP has limited flexibility in the fabrication of complex structures (like hollow and overhanging) due to the difficulties in support preparation using the extruded diluted liquid ink. These restrictions have limited its further application.

Aerosol Jet Printing

Aerosol jet printing (AJP) is a relatively new contactless deposition approach focusing primarily on the fabrication of printed electronics. The raw materials (such as metals, polymers, and ceramics) to be AJP deposited must be in a liquid form and is pneumatic or ultrasonic aerosolized into droplets with a diameter of 1–5 μm. These droplets are then delivered to the substrate by a gas stream to form the desired patterns (Mahajan et al., 2013). A schematic of the AJP process is shown in **Figure 5A**.

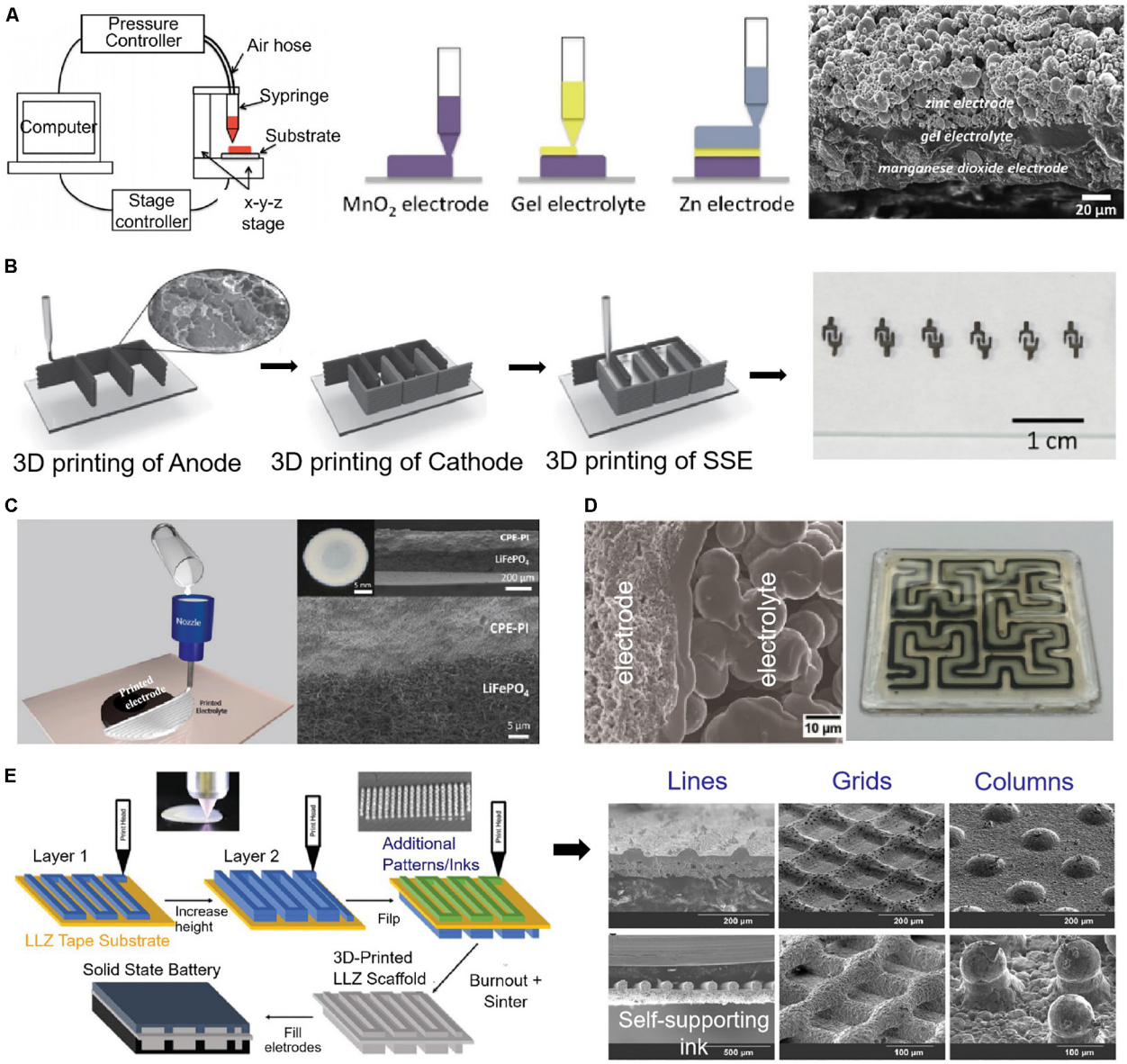

FIGURE 3 | Direct ink writing (DIW). **(A)** Schematic and SEM microscopy of gel electrolyte for Zn-MnO_2 micro-battery. Reproduced from Ho et al. (2010) with permission from IOP Publishing, Ltd. **(B)** Schematic and optical images of polymer electrolyte for $Li_4Ti_5O_{12}$-graphene oxide battery. Reproduced from Fu et al. (2016) with permission from John Wiley & Sons-Books. **(C)** Schematic and SEM micrograph of composite solid electrolyte (CSE) for flexible LIBs ($LiFePO_4$/CSE/$Li_4Ti_5O_{12}$). Reproduced from Blake et al. (2017) with permission from John Wiley & Sons-Books. **(D)** SEM microscopy and optical image of CSE for LIBs with MnO_2 electrode. Reproduced from Cheng et al. (2018) with permission from John Wiley & Sons-Books. **(E)** Scheme and SEM micrographs of $Li_7La_3Zr_2O_{12}$ (LLZ) ceramic electrolyte for Li metal battery (Li/LLZ/Li). Reproduced from Mcowen et al. (2018) with permission from John Wiley & Sons-Books.

The printing resolution of AJP depends not only on the nozzle size but also on the density of the droplets and its interaction with the substrate (Hoey et al., 2012). The AJP is considered as a potential competitor to IJP in the millimeter manufacturing since it allows the non-contact deposition on flexible and 3D non-planar substrates, which is not possible for IJP or DIW technique.

The application of AJP to printing SSEs was first described in the literature by Deiner et al. (2019). This work presented the ink formulation composed of PEO, lithium difluoro(oxalate)borate, and Al_2O_3 nanoparticles suitable for AJP deposition (**Figures 5B–D**). The results showed that the geometry and transport properties of the printed SPEs were mainly sensitive to the chemical identity of the lithium-salt anion and the EO: Li ratio. The LIBs with the AJP deposited SPEs could be discharged at C/15 with capacity >85 mAh g^{-1} at 45°C and 162 mAh g^{-1} at 75°C. Compared with the IJP, the AJP has the following advantages: (i) the extruded inks allow much higher viscosities, larger particle sizes and solid loadings due to the atomization

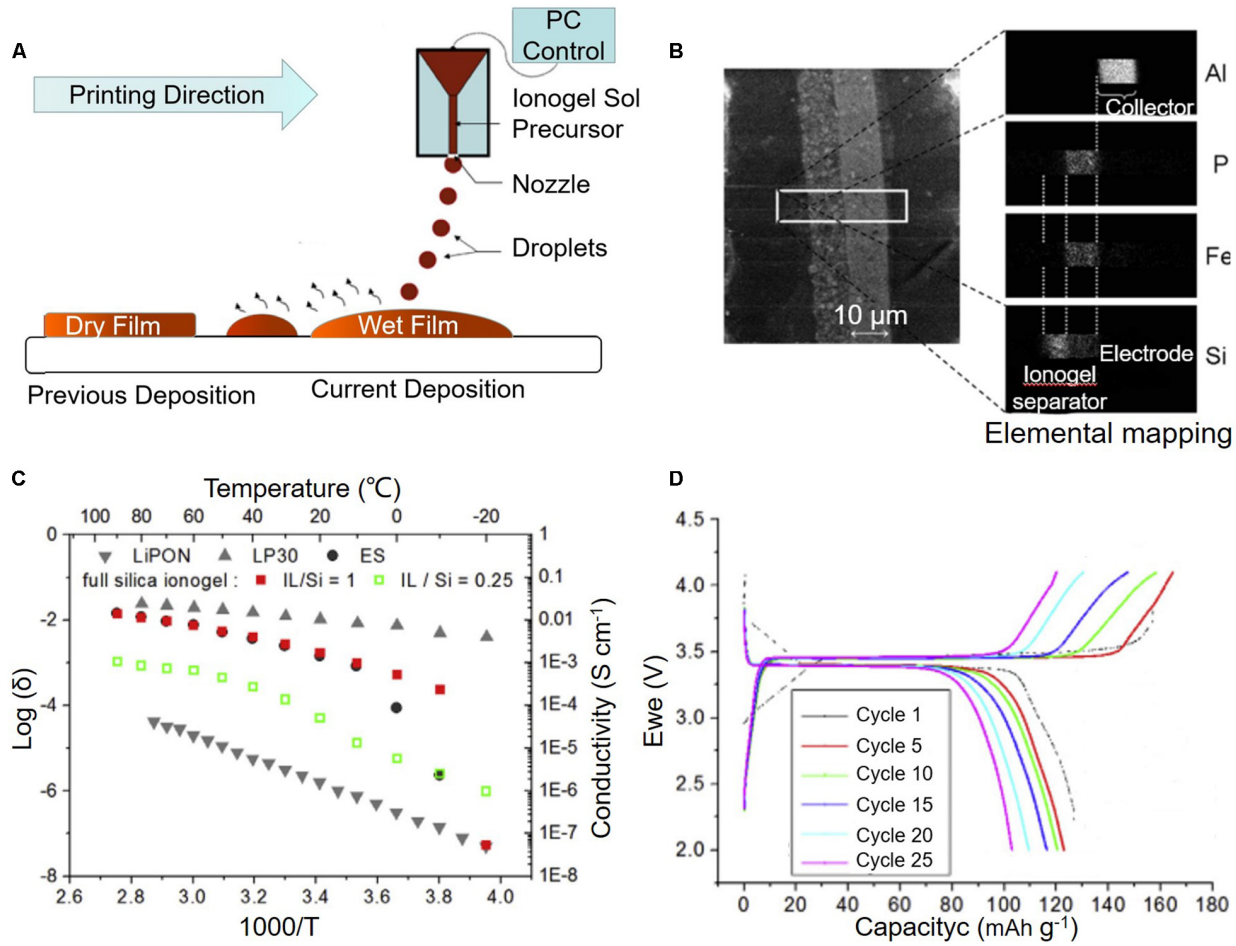

FIGURE 4 | Ink-jet printing (IJP). **(A)** Scheme of the IJP process; **(B)** Cross-section SEM and elemental mapping of porous composite $LiFePO_4$ electrode with printed ionogel electrolytes; **(C)** Temperature-dependent ionic conductivity of the printed ionogels; **(D)** Galvanostatic cycling of half-cell using the printed ionogels and $LiFePO_4$ and $Li_4Ti_5O_{12}$ porous composite electrodes. Reproduced from Delannoy et al. (2015) with permission from Elsevier Science and Technology Journals.

process that reproduces fine droplets, (ii) it is based on the continuous generation of the mist of droplet with a diameter of 1–5 μm, which indicates a higher printing resolution (~5 μm) and deposition speed than in the drop-on-demand IJP process, and (iii) the continuous mist consists of high-density droplets that are tightly focused showing a fine nozzle anti-clogging ability. However, the scalability of the deposition system, especially toward large-area (with build envelope > 3 mm) processing is still challenging for AJP due to its nozzle size and its accessories. Besides, the cost of the additional accessories and focused gas stream in the AJP system is typically high.

Fused Deposition Modeling

Fused deposition modeling (FDM) is a well-known 3D printing technique for creating complex objects in both industry and academia due to its simplicity and affordable machine availability (Bellini and Güçeri, 2003). The forming mechanism of the FDM is similar to that of the DIW which is based on the material-extruded principle, while their feedstock and feeding process is different. A schematic of the FDM process is shown in **Figure 6A**. The FDM printable materials must be solid and thermoplastic in a thin filament shape that can be delivered to an extrusion head by drive wheels. Once extruded from the nozzle, the thermoplastic materials that are heated to their glass transition state would crystallize and solidify to deposit onto the substrate. Common thermoplastic materials used in the FDM technique are Acrylonitrile-butadiene-styrene and polylactic acid (PLA) filaments, in which the PLA has gained increasing popularity due to its environmentally friendly nature. Despite these advantages, the FDM technique has rarely been applied to manufacturing SSEs due to the low ionic conductivity of the thermoplastics. Therefore, the development of filament shaped thermoplastic materials with high ionic conductivity is the key to produce SSEs by FDM.

In 2018, Reyes et al. (2018) first synthesized FDM-printable PLA-based electrolyte filaments with the highest ionic conductivity of 0.031 $mS{\cdot}cm^{-1}$ by infusing a mixture of ethyl methyl carbonate, propylene carbonate, and $LiClO_4$. They also developed the PLA-electrode materials to achieve the 3D printing of full LIBs in arbitrary shapes, such as coin cell

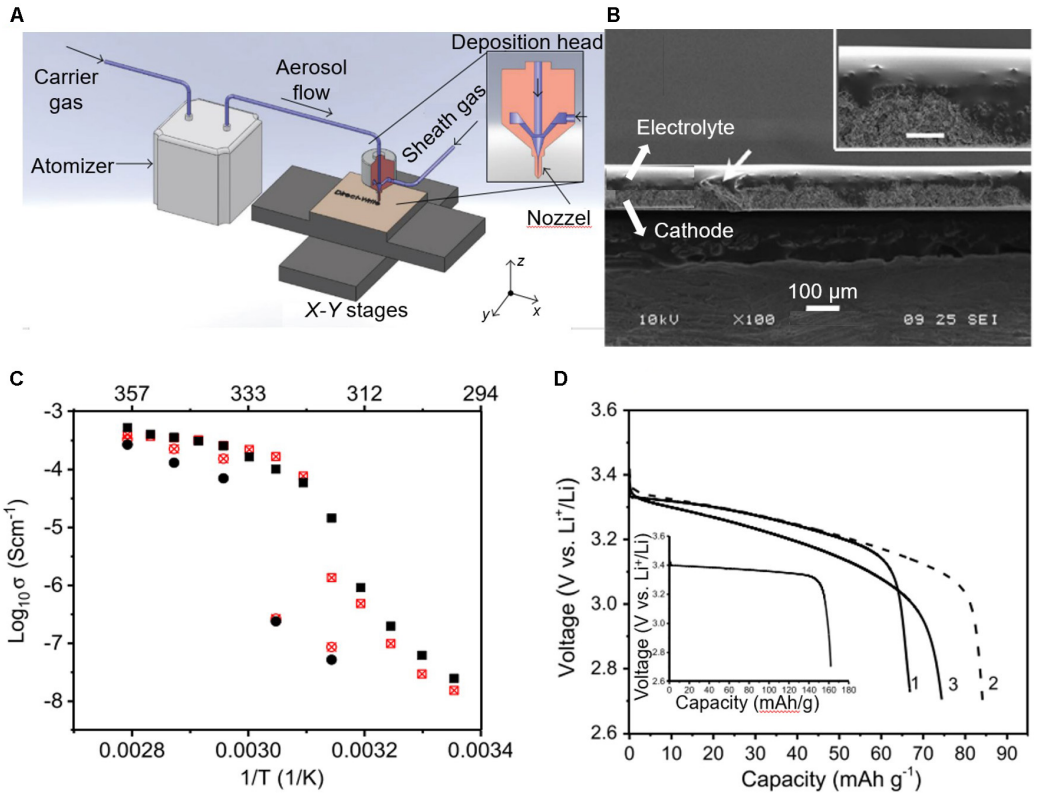

FIGURE 5 | Aerosol jet printing (AJP). **(A)** Scheme of AJP process. Reproduced from Hoey et al. (2012) under the Creative Commons Attribution license. AJP for polyethylene oxide (PEO)-based electrolytes in LIBs with $LiFePO_4$ as cathode: **(B)** Cross-sectional SEM micrograph of the PEO-based electrolytes; **(C)** Temperature-dependent conductivity of the PEO-based electrolytes; **(D)** Discharge curves for batteries created from printed PEO-based electrolyte at 45°C with inset for measurement at 75°C. Reproduced from Deiner et al. (2019) with permission from John Wiley & Sons-Books.

and integrated batteries used in wearable electronic devices as shown in **Figures 6B–E**. However, the printed full cell has a lower Coulombic efficiency (∼88.5% within the first 50 cycles) compared with that of a conventional LIBs (∼95–99%) (Smith et al., 2010). The FDM offers numerous advantages such as low printing cost, large-size capabilities (the maximum build envelope of ∼10 cm), and notably the multi-feedstock structure printability. However, there are still several restrictions on SSE manufacturing by FDM: (i) the printable materials are limited to thermoplastics and must be shaped into filaments, (ii) the thermoplastic filaments must be heated to their glass transition state at a high temperature of 150–180°C, and (iii) the FDM printing resolution along with the *Z*-axis is ranging from 50 to 200 μm, leading to the poor surface quality and structure controllability.

Lithography-Based 3D Printing of Solid-State Electrolytes

Stereolithography

Stereolithography (SL) is considered as the most prominent and popular 3D printing technique and has been applied for the fabrication of polymer, ceramic, and glass parts (Eckel et al., 2016; Ngo et al., 2018; Santoliquido et al., 2019). A schematic of the SL process is shown in **Figure 7A**. SL enables the manufacturing of complex 3D micro-lattices by selectively polymerizing and solidifying the photocurable resin using a light source of a certain wavelength (usually in the UV range) (Chartrain et al., 2018). The polymerization process generally proceeds on the liquid surface. Once one layer of polymerization is completed, the vat or platform supporting the building part is lifted or lowered the thickness of a layer. Sometimes, a blade is required to level off the liquid surface before polymerizing the next layer. The SL photocurable resin consists of mainly photo-active monomers and other additives in very small amounts, particularly the photoinitiator (Manapat et al., 2017). Compared with the DW-based 3D printing technique (e.g., DIW, IJP, AJP, and FDM), SL is capable of fabricating arbitrary 3D geometries including various hollow carved features of fine resolutions down to the micrometer scale, and it can eliminate the restrictions from toolpath and serial extrusion (Yang et al., 2016). Therefore, the SL has a high potential for the fabrication of various types of SSEs, including SPEs, CSEs, and ISEs.

In 2015, Kim S.H. et al. (2015) prepared SPE layer and SPE matrix-embedded electrodes on arbitrary objects and then assemble into multilayer-structured flexible LIBs in various form factors (**Figure 7B**). The printed batteries presented a good long-term charge storage capability and a medium level of volumetric

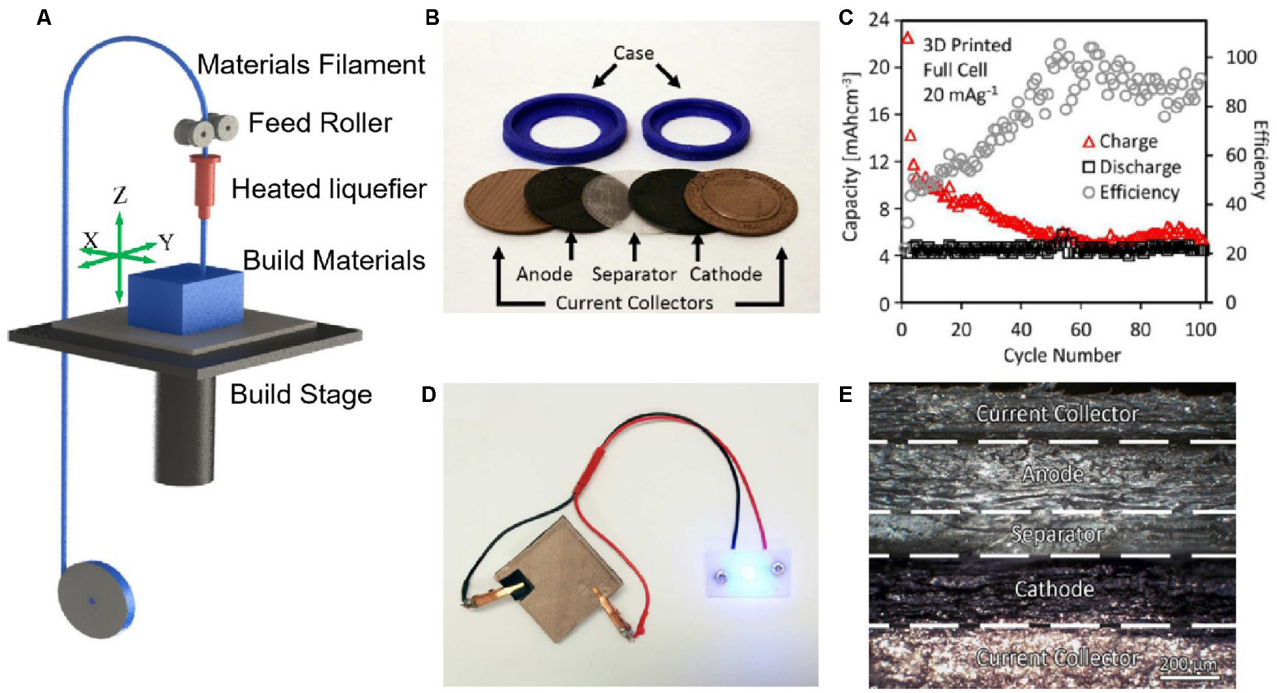

FIGURE 6 | Fused deposition modeling (FDM). **(A)** Scheme of FDM process. Reproduced from Klippstein et al. (2018) with permission from John Wiley & Sons-Books. FDM for polylactic acid (PLA)-based electrolytes in LIBs (lithium titanate/PLA matrix/lithium manganese oxide): **(B)** Individual components of the 3D printed coin cell; **(C)** The capacity and coulombic efficiency at a current density of 20 mAg^{-1} for 100 cycles; **(D)** Optical image of the printed battery powering an LED; **(E)** SEM cross-section of the single print battery. Reproduced from Reyes et al. (2018) with permission from American Chemical Society.

energy density. Chen Q. et al. (2017) developed a UV-curable Poly (ethylene glycol)-based resin for SL printing a 3D gel polymer electrolyte for micro LIBs in a low-cost and high-throughput way. As shown in **Figure 7C**, the printed zigzag-shaped GPE could increase the contact area with electrodes, and an improved ionic conductivity of 4.8×10^{-3} S cm^{-1} can be obtained at ambient temperature, which is comparable to that of liquid electrolyte. Zekoll et al. (2018) reported an SL-printed CSEs comprising 3D bicontinuous $Li_{1.4}Al_{0.4}Ge_{1.6}(PO_4)_3$ (LAGP) ceramic electrolyte and an insulating polymer (epoxy polymer, polypropylene) for Li metal battery (**Figure 7D**). This method could precisely control the ceramic to polymer ratio, and the geometry and size of a diverse range of precise microarchitectures, such as cubic, gyroidal, diamond, and bijel-derived structures. The gyroid LAGP-epoxy electrolyte had an ionic conductivity of 1.6×10^{-4} S cm^{-1}, which was on the same order of magnitude as a LAGP pellet, while the printed electrolyte demonstrated up to 28% higher compressive strength and up to five times the flexural strength. A recent work reported by Pesce et al. (2020) developed self-supported all-ceramic electrolytes of 8 mol% yttria-stabilized zirconia (YSZ) for the solid oxide fuel cell (SOFC) printed by SL (**Figure 7E**). The printed dense and crack-free 8YSZ electrolytes reached an ionic conductivity as high as 3.0×10^{-2} S cm^{-1} at 800°C in the planar and corrugated geometries. The SL printed corrugated YSZ electrolytes presented an increase of 57% in power density (410 mW cm^{-2} at 900°C) compared with conventional SOFC technology, which was mainly due to high-aspect-ratio geometrical aspects. The SL has demonstrated numerous advantages, such as high printing resolution (10–100 μm) and surface quality. Besides, SL has great potential in the preparation of SSEs for multi-scale batteries, particularly the micron-scale battery. However, the availability of SL printable photosensitive resins or precursor polymers is limited and costly (around $100/kg for photosensitive resins and more expensive for precursors), and manual supports are required for printing hollow or overhanging structures.

Digital Light Processing

Digital light processing (DLP) is a mask-based SL technique using a digital micromirror device (DMD) to project a mask of light that serves to solidify a whole layer in a few seconds (Chartrain et al., 2018). The forming mechanism and feedstock of the DLP are similar to the SL. A schematic of the DLP process is shown in **Figure 8A**. In the DLP system, the DMD is an array of up to several millions of microscopically small mirrors on a semiconductor chip, and each mirror represents one or more pixels in the projected image (Han et al., 2019). In this case, the printing resolution of the DLP is related to the number of mirrors in DMD. The layer-like solidification in the DLP offers numerous advantages over the SL point-by-point scanning process: (i) the build times are much reduced as they mainly depend on the layer thickness and exposure time, and (ii) the residual stress of DLP samples is small since no difference exists between the outline and inner area during layer solidification. These advantages have

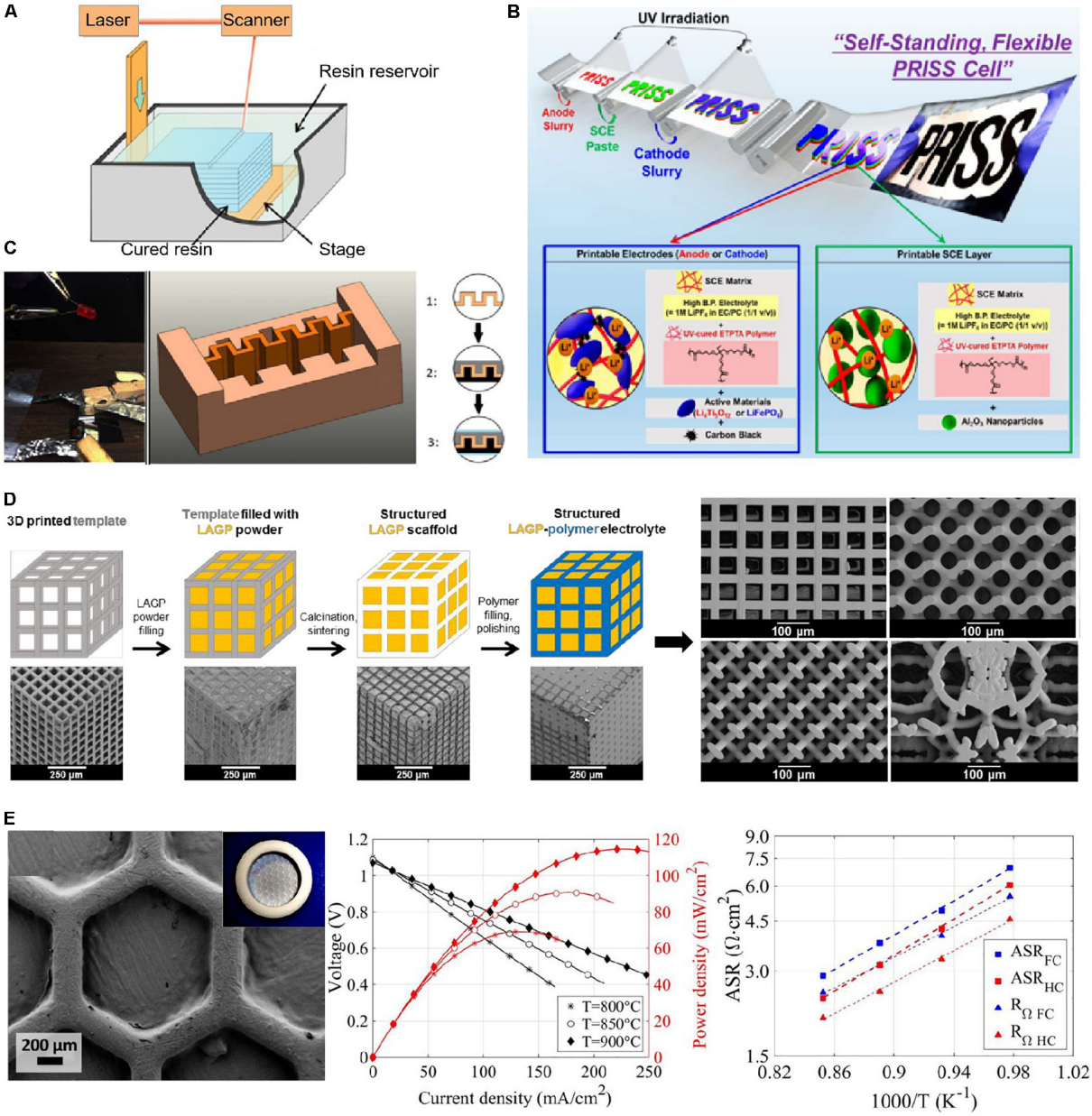

FIGURE 7 | Stereolithography (SL). **(A)** Scheme of SL process. Reproduced from Gross et al. (2014) with permission from American Chemical Society. SL for solid-state electrolytes (SSEs): **(B)** UV curing-assisted stencil printing process of solid polymer electrolytes (SPEs, = ethoxylated trimethylolpropane triacrylate monomer/high boiling point electrolyte/Al_2O_3 nanoparticles) thin layer for LIBs [$LiFePO_4$ (LFP)/SPE/$Li_4Ti_5O_{12}$ (LTO)]. Reproduced from Kim S.H. et al. (2015) with permission from American Chemical Society. **(C)** Optical image and 3D structure of Poly (ethylene glycol)-based SPE for micro LIBs (LFP/SPE/LTO). Reproduced from Chen Q. et al. (2017) with permission from IOP Publishing, Ltd. **(D)** Schematic and SEM images of the 3D printed templates with the cube, gyroid, diamond and bijel-derived microarchitectures of $Li_{1.4}Al_{0.4}Ge_{1.6}(PO_4)_3$ (LAGP)-epoxy electrolytes for Li metal battery with symmetric lithium electrodes. Reproduced from Zekoll et al. (2018) with permission from Royal Society of Chemistry. **(E)** Optical image, SEM images, and voltage-/power- current density curves of lanthanum strontium manganite (LSM-YSZ)/YSZ/Ni–YSZ solid oxide cells. Reproduced from Pesce et al. (2020) under a Creative Commons Attribution 3.0 Unported License-Published by The Royal Society of Chemistry.

attracted considerable attention for fabricating dense ceramics in a variety of fields, including ceramic electrolytes for SOFCs.

The most recent work on ceramic electrolyte manufacturing by DLP was carried out by Xing et al. (2020). To enhance the performance of SOFCs, the fully dense 8mol% YSZ electrolyte was designed with ripple shapes and prepared by DLP with different printing angles (0°, 15°, 30°, 45°) (**Figures 8B,C**). This printed special electrolyte could increase the electrode-electrolyte interface by ∼36%, and thus enhancing the power density by ∼32% at a test temperature of 800°C and by ∼37% at

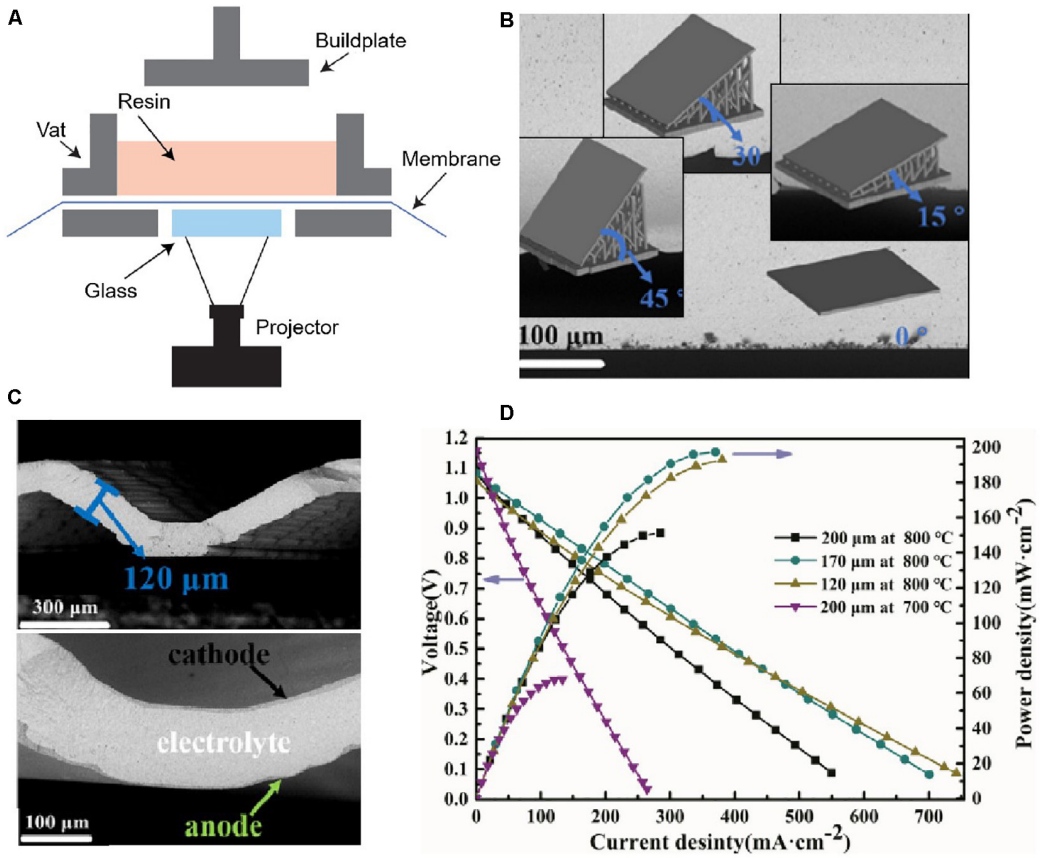

FIGURE 8 | Digital light processing (DLP). **(A)** Scheme of DLP process. Reproduced from Luongo et al. (2020) with permission from John Wiley & Sons-Books. DLP for fully dense 8 mol% yttria-stabilized zirconia (8YSZ) electrolyte in Solid Oxide Fuel Cell (NiO-8YSZ/8YSZ/$La_{0.8}Sr_{0.2}MnO_3$): **(B)** SEM images of printed YSZ with different angles; **(C)** SEM images of ripple-shaped YSZ; **(D)** Voltage- and power- current density curves of the full ripple-shaped cells. Reproduced from Xing et al. (2020) with permission from Elsevier Science & Technology Journals.

700°C compared with that of the reference flat cell (**Figure 8D**). This work has demonstrated the potential for manufacturing specific patterned SSE by DLP, for the fabrication of SOFCs with improved and predictable performance. The DLP has a comparable printing resolution (10–100 μm) and surface quality to SL, but much-reduced build time and less residual stress that can manufacture high-reliable SSEs in a high-efficiency way. However, the costly photosensitive resins/precursors and manual supports are still challenges faced by DLP.

In recent years, multiple lithography-based 3D printing techniques have been developed, such as two-photon polymerization (TPP) (Truby and Lewis, 2016), continuous liquid interface production (CLIP) (Tumbleston et al., 2015) and projection micro stereolithography (PμSL) (Park et al., 2012), all have the potential to achieve a comparable or higher printing resolution than 10–100 μm (**Figure 9**). CLIP has a printing resolution of 50∼100 μm, while the parts can be directly drawn out of the resin in minutes using an oxygen-permeable window (Tumbleston et al., 2015). PμSL can achieve a printing resolution of 2∼8.5 μm using a 3-D grayscale DMD as a dynamic mask and a demagnifying lens system as the spatial light modulator (Sun et al., 2005). In particular, TPP enables the creation of feature size less than 1 μm by the simultaneous absorption of two photons of a near-infrared (780 nm) or green (515 nm) laser (Obata et al., 2013). This lithography-based 3D printing technique has a high potential for the fabrication of SSEs with fine features from hundreds of nanometers to microns.

CONCLUSION AND PERSPECTIVES

In this review, we have first discussed the general processes and limitations of the traditional methods to manufacture SSEs. Then, through a comprehensive overview of two large groups of 3D printing techniques that are either based on DW or SL, we pointed out the advantages of novel 3D printing techniques over the traditional SSE manufacturing methods from the aspects of building mechanisms, feedstock selection, build envelope, printing resolution, and application (nano-scaled, flexible, and large-scale battery grids). We emphasized the prospects and feasibility of manufacturing SSEs using lithography-based 3D printing to overcome the technical barriers and improve the compatibility of solid-solid interfaces. Finally, we discussed several existing challenges associated with the

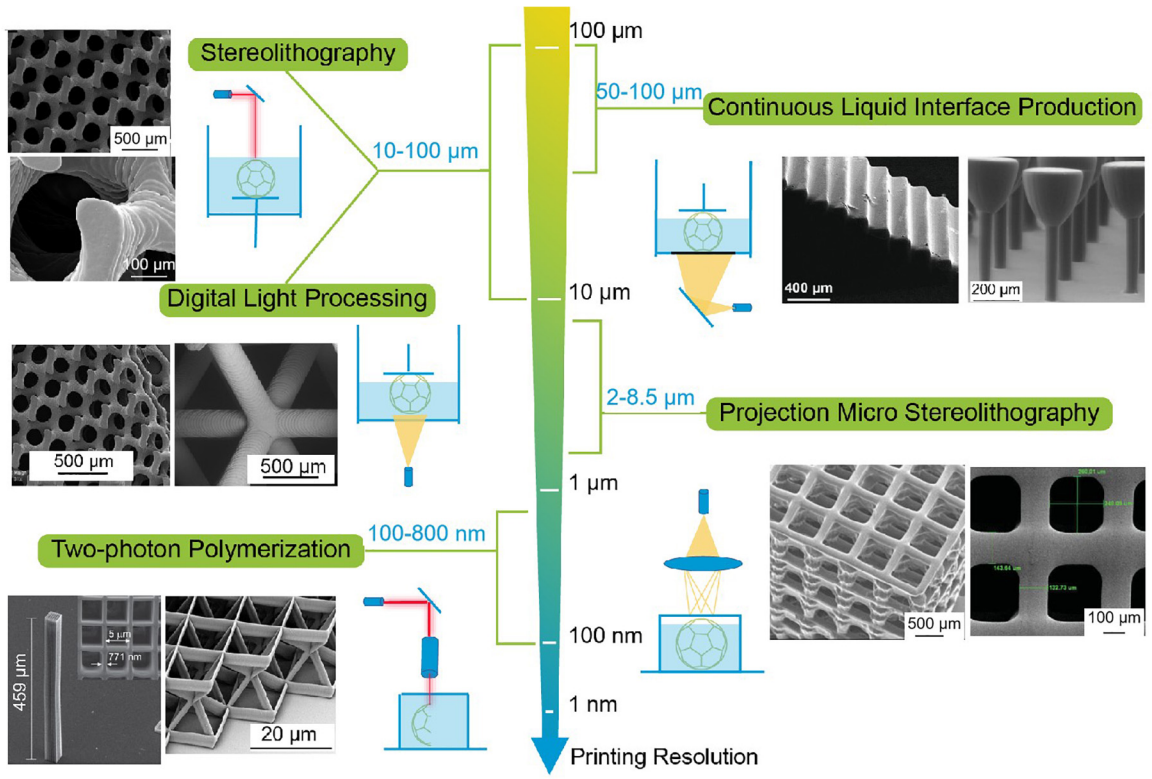

FIGURE 9 | Printing resolution comparison of lithography-based 3D printing technique [stereolithography (SL), digital light processing (DLP), continuous liquid interface production (CLIP), projection micro stereolithography (PμSL), and two-photon polymerization (TPP)]. SL reproduced from Jansen et al. (2009) with permission from American Chemical Society. DLP reproduced from Lee et al. (2007) with permission from American Chemical Society. CLIP reproduced from Tumbleston et al. (2015) with permission from American Association for the Advancement of Science. PμSL reproduced from Lee et al. (2008) with permission from John Wiley & Sons-Books. TPP reproduced from Obata et al. (2013) under the Creative Commons license.

3D printing process and the corresponding future perspectives toward better addressing those challenges, aiming to provide guidance that would drive the development of 3D printing techniques more closely oriented with battery manufacturing. Overall, behind the evolution of batteries, the steady driving force has always been the continuously maturing and advancing manufacturing techniques.

Given the advantages of high printing resolution, flexible preparation of highly complex structures, and broad feedstock selections, the 3D printing technique has demonstrated their great potential to produce various types and form factors of SSEs. However, there are still several challenges that should be addressed as follow: (i) the challenges in manufacturing for air/moisture sensitive SSEs. Most of the 3D printing technique uses a feedstock in a liquid or ink form, such as DIW, IJP, and AJP, (ii) the limitations in high-resolution (down to nanoscale) manufacturing. For example, the nano-LIB for biomedical applications and the nanometer comb-shaped SSEs for reducing internal resistance, (iii) the challenges in manufacturing SSEs for grid-scale applications. For example, the SOFCs and large-scale battery grids for renewable energy storage, and (iv) the potential issues in post-treatment for ISEs. For example, the stress, cracks, Li volatility, and side reaction are easily caused during time-consuming (debinding or sintering) (Nyman et al., 2010; Pfenninger et al., 2019). To address the above challenges, further efforts are highly recommended in the following aspects: (i) integrate the 3D printing technique and traditional battery manufacturing to promote the development of high energy density all-solid-state batteries, (ii) push the printing resolution down to nanometer with novel nanotechnologies, (iii) develop the industrial-level printers or conveyor-like printing platform to manufacture SSEs for grid-scale applications, and (iv) combine some innovative sintering technologies that are compatible with 3D-printed complex parts.

This review has demonstrated the feasibility of manufacturing SSEs by 3D printing, but more efforts are required to fully bridge the gap between current technological capabilities and future manufacturing requirements. Although 3D printing offers unprecedented flexibility in adjusting SSE's structural dimensionality and complexity comparing to the traditional methods, it must not be mistaken as the omnipotent solution to many inherent obstacles in battery manufacturing. To realize a greater potential of applying 3D printing in battery manufacturing requires multidisciplinary joint effort. As from a perspective of materials science, further experimental and computational studies are needed systematically to explore

the SSE's composition-structure-property relations. For which should contribute to fulfill higher current densities and better mechanical/chemical stabilities of the battery cell. Digging deeper into the reaction mechanisms from an electrochemical perspective, one could investigate and optimize the ion transport kinetics at the electrode/electrolyte interfaces to enhance the transfer efficiency of the conducting ion. Through a more comprehensive design in mechanical engineering, one could integrate special accommodations for air/moisture sensitive samples into existing instrumental setups of 3D printing to allow a wider materials selection. Overall, 3D printing technology has utilized many advantages observed from the traditional manufacturing methods over many years. With the joint effort of the multidisciplinary studies, 3D printing is optimistic to soon realize its full potential in manufacturing SSEs. We believe that the wide adoption of 3D printing technologies should not only focus on the manufacturing process, but also draw inspiration from disciplines such as surface chemistry, materials science and mechanical engineering. For example, the limited availability and costly of printable photosensitive resins or precursor polymers (above $100 per kilogram) for SL will force us to develop novel SL printable materials with low cost, and wide material compatibility. The poor interface compatibility of solid/solid interface will push us to explore the surface modification and structural design of SSEs with strong inter-particle interaction and low interface impedance. Besides, some special requirements (such as inert atmosphere and dry environment) will force us to develop specific 3D printing technique for the battery manufacturing. Therefore, the application of SSE 3D printing in the future requires the joint development of multiple disciplines such as surface chemistry, material science and mechanical engineering.

AUTHOR CONTRIBUTIONS

FS and YS: conception or design of the work and critical revision of the article. AC and CQ: drafting the article. All authors contributed to the article and approved the submitted version.

FUNDING

FS acknowledges the start-up fund support from the Department of Energy and Mineral Engineering at Penn State University.

REFERENCES

Abetti, P. A. (1952). The letters of Alessandro Volta. *Electr. Eng.* 71, 773–776. doi: 10.1109/ee.1952.6437680

Ambrosi, A., and Pumera, M. (2016). 3D-printing technologies for electrochemical applications. *Chem. Soc. Rev.* 45, 2740–2755. doi: 10.1039/c5cs00714c

Appetecchi, G. B., Alessandrini, F., Carewska, M., Caruso, T., Prosini, P. P., Scaccia, S., et al. (2001). Investigation on lithium–polymer electrolyte batteries. *J. Power Sources* 97, 790–794.

Bellini, A., and Güçeri, S. (2003). Mechanical characterization of parts fabricated using fused deposition modeling. *Rapid Prototyp. J.* 9, 252–264. doi: 10.1108/13552540310489631

Blake, A. J., Kohlmeyer, R. R., Hardin, J. O., Carmona, E. A., Maruyama, B., Berrigan, J. D., et al. (2017). 3D printable ceramic-polymer electrolytes for flexible high-performance Li-ion batteries with enhanced thermal stability. *Adv. Energy Mater.* 7:1602920. doi: 10.1002/aenm.201602920

Blanga, R., Burstein, L., Berman, M., Greenbaum, S. G., and Golodnitsky, D. (2015). Solid polymer-in-ceramic electrolyte formed by electrophoretic deposition. *J. Electrochem. Soc.* 162, D3084–D3089.

Braam, K. T., Volkman, S. K., and Subramanian, V. (2012). Characterization and optimization of a printed, primary silver–zinc battery. *J. Power Sources* 199, 367–372. doi: 10.1016/j.jpowsour.2011.09.076

Buchmann, I. (2001). *Batteries in a Portable World: A Handbook on Rechargeable Batteries for Non-Engineers*. Richmond: Cadex Electronics.

Carli, M. D., Caso, M. F., Aurora, A., Seta, L. D., and Prosini, P. P. (2019). "Electrospinning nanofibers as separators for lithium-ion batteries", in: Proceedings of the *15th International Conference on Concentrator Photovoltaic Systems (CPV-15)*, Melville, NY.

Cavaliere, S., Subianto, S., Savych, I., Jones, D. J., Roziere, J. J. E., and Science, E. (2011). Electrospinning: designed architectures for energy conversion and storage devices. *Energy Environ. Sci.* 4, 4761–4785. doi: 10.1039/c1ee02201f

Chang, P., Mei, H., Zhou, S., Dassios, K. G., and Cheng, L. (2019). 3D printed electrochemical energy storage devices. *J. Mater. Chem. A* 7, 4230–4258. doi: 10.1039/c8ta11860d

Chartrain, N. A., Williams, C. B., and Whittington, A. R. (2018). A review on fabricating tissue scaffolds using vat photopolymerization. *Acta Biomater.* 74, 90–111. doi: 10.1016/j.actbio.2018.05.010

Chen, A.-N., Li, M., Wu, J.-M., Cheng, L.-J., Liu, R.-Z., Shi, Y.-S., et al. (2019). Enhancement mechanism of mechanical performance of highly porous mullite ceramics with bimodal pore structures prepared by selective laser sintering. *J. Alloys Compd.* 776, 486–494. doi: 10.1016/j.jallcom.20180.10337

Chen, A.-N., Li, M., Xu, J., Lou, C.-H., Wu, J.-M., Cheng, L.-J., et al. (2018). High-porosity mullite ceramic foams prepared by selective laser sintering using fly ash hollow spheres as raw materials. *J. Eur. Ceram. Soc.* 38, 4553–4559. doi: 10.1016/j.jeurceramsoc.2018.05.031

Chen, A.-N., Wu, J.-M., Cheng, L.-J., Liu, S.-J., Ma, Y.-X., Li, H., et al. (2020). Enhanced densification and dielectric properties of CaTiO3-0.3NdAlO3 ceramics fabricated by direct coagulation casting. *J. Eur. Ceram. Soc.* 40, 1174–1180. doi: 10.1016/j.jeurceramsoc.2019.12.033

Chen, A.-N., Wu, J.-M., Liu, K., Chen, J.-Y., Xiao, H., Chen, P., et al. (2017). High-performance ceramic parts with complex shape prepared by selective laser sintering: a review. *Adv. Appl. Ceram.* 117, 100–117. doi: 10.1080/17436753.2017.1379586

Chen, C., Yu, T., Yang, M., Zhao, X., and Shen, X. (2019). An all-solid-state rechargeable chloride ion battery. *Adv. Sci.* 6:1802130. doi: 10.1002/advs.201802130

Chen, Q., Xu, R., He, Z., Zhao, K., and Pan, L. (2017). Printing 3D gel polymer electrolyte in Lithium-ion microbattery using stereolithography. *J. Electrochem. Soc.* 164, A1852–A1857.

Chen, W., Lei, T., Wu, C., Deng, M., Gong, C., Hu, K., et al. (2018). Designing safe electrolyte systems for a high-stability Lithium-Sulfur battery. *Adv. Energy Mater.* 8:1702348. doi: 10.1002/aenm.201702348

Chen, Y., Zhuo, S., Li, Z., and, Wang, C. (2020). Redox polymers for rechargeable metal-ion batteries. *EnergyChem* 2:100030. doi: 10.1016/j.enchem.2020.100030

Chen, Z., Li, Z., Li, J., Liu, C., Lao, C., Fu, Y., et al. (2019). 3D printing of ceramics: a review. *J. Eur. Ceram. Soc.* 39, 661–687.

Cheng, M., Deivanayagam, R., and Shahbazian-Yassar, R. (2020). 3D printing of electrochemical energy storage devices: a review of printing techniques and electrode/electrolyte architectures. *Batter. Supercaps* 3, 130–146. doi: 10.1002/batt.201900130

Cheng, M., Jiang, Y., Yao, W., Yuan, Y., Deivanayagam, R., Foroozan, T., et al. (2018). Elevated-temperature 3D printing of hybrid solid-state electrolyte for Li-ion batteries. *Adv. Mater.* 30:e1800615.

Choi, Y. E., Park, K. H., Kim, D. H., Oh, D. Y., Kwak, H. R., Lee, Y. G., et al. (2017). Coatable Li4SnS4 solid electrolytes prepared from aqueous solutions for all-solid-state Lithium-ion batteries. *ChemSusChem* 10, 2605–2611. doi: 10.1002/cssc.201700409

Commarieu, B., Paolella, A., Daigle, J.-C., and Zaghib, K. (2018). Toward high lithium conduction in solid polymer and polymer–ceramic batteries. *Curr. Opin. Electrochem.* 9, 56–63. doi: 10.1016/j.coelec.2018.03.033

Cousseau, J.-F., Siret, C., Biensan, P., and Broussely, M. (2006). Recent developments in Li-ion prismatic cells. *J. Power Sources* 162, 790–796. doi: 10.1016/j.jpowsour.2005.02.095

Deiner, L. J., Jenkins, T., Howell, T., and Rottmayer, M. (2019). Aerosol jet printed polymer composite electrolytes for solid-state Li-ion batteries. *Adv. Eng. Mater.* 21:1900952. doi: 10.1002/adem.201900952

Delannoy, P. E., Riou, B., Lestriez, B., Guyomard, D., Brousse, T., and Le Bideau, J. (2015). Toward fast and cost-effective ink-jet printing of solid electrolyte for lithium microbatteries. *J. Power Sources* 274, 1085–1090. doi: 10.1016/j.jpowsour.2014.10.164

Deng, Z., Jiang, H., Hu, Y., Liu, Y., Zhang, L., Liu, H., et al. (2017). 3D ordered macroporous MoS2@ C nanostructure for flexible Li-ion batteries. *Adv. Mater.* 29:1603020. doi: 10.1002/adma.201603020

Derby, B. (2010). Inkjet printing of functional and structural materials: fluid property requirements, feature stability, and resolution. *Annu. Rev. Mater. Res.* 40, 395–414. doi: 10.1146/annurev-matsci-070909-104502

Diouf, B., and Pode, R. (2015). Potential of lithium-ion batteries in renewable energy. *Renew. Energy* 76, 375–380. doi: 10.1016/j.renene.2014.11.058

Dirican, M., Yan, C., Zhu, P., and Zhang, X. (2019). Composite solid electrolytes for all-solid-state lithium batteries. *Mater. Sci. Eng. R Rep.* 136, 27–46.

Dobrozhan, O., Pshenychnyi, R., Vorobiov, S., Kurbatov, D., Komanicky, V., and Opanasyuk, A. (2020). Influence of the thermal annealing on the morphological and structural properties of ZnO films deposited onto polyimide substrates by ink-jet printing. *SN Appl. Sci.* 2:365.

Du, C.-F., Liang, Q., Luo, Y., Zheng, Y., and Yan, Q. (2017). Recent advances in printable secondary batteries. *J. Mater. Chem. A* 5, 22442–22458. doi: 10.1039/c7ta07856k

Dudney, N. J. (2008). Thin film micro-batteries. *Electrochem. Soc. Interface* 17, 44–48.

Dunn, B., Farrington, G. C., and Katz, B. (1994). Sol-gel approaches for solid electrolytes and electrode materials. *Solid State Ion.* 70, 3–10. doi: 10.1016/0167-2738(94)90281-x

Eckel, Z. C., Zhou, C., Martin, J. H., Jacobsen, A. J., Carter, W. B., and Schaedler, T. A. J. S. (2016). Additive manufacturing of polymer-derived ceramics. *Science* 351, 58–62. doi: 10.1126/science.aad2688

Fergus, J. W. (2010). Ceramic and polymeric solid electrolytes for lithium-ion batteries. *J. Power Sources* 195, 4554–4569. doi: 10.1016/j.jpowsour.2010.01.076

Franks, G. V., Tallon, C., Studart, A. R., Sesso, M. L., and Leo, S. (2017). Colloidal processing: enabling complex shaped ceramics with unique multiscale structures. *J. Am. Ceram. Soc.* 100, 458–490. doi: 10.1111/jace.14705

Fritzler, K. B., and Prinz, V. Y. J. P. U. (2017). 3D printing methods for micro- and nanostructures. *Phys. Uspekhi.* 62, 54–69. doi: 10.3367/ufne.2017.11.038239

Fu, K., Wang, Y., Yan, C., Yao, Y., Chen, Y., Dai, J., et al. (2016). Graphene oxide-based electrode inks for 3D-printed Lithium-ion batteries. *Adv. Mater.* 28, 2587–2594. doi: 10.1002/adma.201505391

Fujimoto, D., Kuwata, N., Matsuda, Y., Kawamura, J., and Kang, F. (2015). Fabrication of solid-state thin-film batteries using LiMnPO 4 thin films deposited by pulsed laser deposition. *Thin Solid Films* 579, 81–88. doi: 10.1016/j.tsf.2015.02.041

Furukawa, N., Inoue, K., and Murakami, S. (1984). *Alkaline Battery*. Google Patents.

Gelfond, N. V., Bobrenok, O. F., Predtechensky, M. R., Morozova, N. B., Zherikova, K. V., and Igumenov, I. K. (2009). Chemical vapor deposition of electrolyte thin films based on yttria-stabilized zirconia. *Inorg. Mater.* 45, 659–665.

Goodenough, J. B., and Singh, P. (2015). Review—solid electrolytes in rechargeable electrochemical cells. *J. Electrochem. Soc.* 162, A2387–A2392.

Greatbatch, W., and Holmes, C. F. (1991). History of implantable devices. *IEEE Eng. Med. Biol. Mag.* 10, 38–41.

Gross, B. C., Erkal, J. L., Lockwood, S. Y., Chen, C., and Spence, D. M. J. A. C. (2014). Evaluation of 3D printing and its potential impact on biotechnology and the chemical sciences. 86, 3240–3253. doi: 10.1021/ac403397r

Hafner, S., Guthrey, H., Lee, S.-H., and Ban, C. (2019). Synchronized electrospinning and electrospraying technique for manufacturing of all-solid-state lithium-ion batteries. *J. Power Sources* 431, 17–24. doi: 10.1016/j.jpowsour.2019.05.008

Han, T., Kundu, S., Nag, A., and Xu, Y. (2019). 3D printed sensors for biomedical applications: a review. *Sensors* 19:1706. doi: 10.3390/s19071706

Hayashi, A., Ohtomo, T., Mizuno, F., Tadanaga, K., and Tatsumisago, M. (2003). All-solid-state Li/S batteries with highly conductive glass–ceramic electrolytes. *Electrochem. Commun.* 5, 701–705. doi: 10.1016/s1388-2481(03)00167-x

Hayashi, A., Yamashita, H., Tatsumisago, M., and Minami, T. (2002). Characterization of Li2S–SiS2–LixMOy (M = Si, P, Ge) amorphous solid electrolytes prepared by melt-quenching and mechanical milling. *Solid State Ion.* 148, 381–389. doi: 10.1016/s0167-2738(02)00077-2

He, P., Chen, Q., Yan, M., Xu, X., Zhou, L., Mai, L., et al. (2019). Building better Zinc-ion batteries: a materials perspective. *EnergyChem* 1:100022. doi: 10.1016/j.enchem.2019.100022

Hench, L. L., and West, J. K. (1990). The sol-gel process. *Chem. Rev.* 90, 33–72.

Hitz, G. T., Mcowen, D. W., Zhang, L., Ma, Z., Fu, Z., Wen, Y., et al. (2019). High-rate lithium cycling in a scalable trilayer Li-garnet-electrolyte architecture. *Mater. Today* 22, 50–57. doi: 10.1016/j.mattod.2018.04.004

Ho, C. C., Evans, J. W., and Wright, P. K. (2010). Direct write dispenser printing of a Zinc microbattery with an ionic liquid gel electrolyte. *J. Micromech. Microeng.* 20:104009. doi: 10.1088/0960-1317/20/10/104009

Hoey, J. M., Lutfurakhmanov, A., Schulz, D. L., and Akhatov, I. S. (2012). A Review on Aerosol-based direct-write and its applications for microelectronics. *J. Nanotechnol.* 2012, 1–22. doi: 10.1155/2012/324380

Jansen, J., Melchels, F. P. W., Grijpma, D. W., and Feijen, J. J. B. (2009). Fumaric acid monoethyl ester-functionalized poly(D,L-Lactide)/N-vinyl-2- pyrrolidone Resins for the preparation of tissue engineering scaffolds by stereolithography. *Biomacromolecules* 10, 214–220. doi: 10.1021/bm801001r

Jiang, Z., Wang, S., Chen, X., Yang, W., Yao, X., Hu, X., et al. (2020). Tape-casting Li0.34La0.56TiO3 ceramic electrolyte films permit high energy density of Lithium-metal batteries. *Adv. Mater.* 32:1906221. doi: 10.1002/adma.201906221

Johannessen, E. A., Wang, L., Wyse, C., Cumming, D. R., and Cooper, J. M. (2006). Biocompatibility of a lab-on-a-pill sensor in artificial gastrointestinal environments. *IEEE Trans. Biomed. Eng.* 53, 2333–2340. doi: 10.1109/tbme.2006.883698

Judez, X., Zhang, H., Li, C., Eshetu, G. G., González-Marcos, J. A., Armand, M., et al. (2017). Review—solid electrolytes for safe and high energy density Lithium-Sulfur batteries: promises and challenges. *J. Electrochem. Soc.* 165, A6008–A6016.

Jung, G. B., Huang, T., Huang, M. H., and Chang, C. L. J. J. O. M. S. (2001). Preparation of samaria-doped ceria for solid-oxide fuel cell electrolyte by a modified sol-gel method. *J. Mater. Sci.* 36, 5839–5844.

Kim, J. G., Son, B., Mukherjee, S., Schuppert, N., Bates, A., Kwon, O., et al. (2015). A review of lithium and non-lithium based solid state batteries. *J. Power Sources* 282, 299–322.

Kim, S. H., Choi, K. H., Cho, S. J., Choi, S., Park, S., and Lee, S. Y. (2015). Printable solid-state Lithium-ion batteries: a new route toward shape-conformable power sources with aesthetic versatility for flexible electronics. *Nano Lett.* 15, 5168–5177. doi: 10.1021/acs.nanolett.5b01394

Klippstein, H., Diaz De Cerio Sanchez, A., Hassanin, H., Zweiri, Y., and Seneviratne, L. (2018). Fused deposition modeling for Unmanned Aerial Vehicles (UAVs): a review. *Adv. Eng. Mater.* 20:1700552. doi: 10.1002/adem.201700552

Kotobuki, M., Koishi, M., and Kato, Y. (2013). Preparation of Li1.5Al0.5Ti1.5(PO4)3 solid electrolyte via a co-precipitation method. *Ionics* 19, 1945–1948. doi: 10.1007/s11581-013-1000-4

Kurzweil, P. (2010). Gaston Planté and his invention of the lead–acid battery—the genesis of the first practical rechargeable battery. *J. Power Sources* 195, 4424–4434. doi: 10.1016/j.jpowsour.2009.12.126

Lau, J., Deblock, R. H., Butts, D. M., Ashby, D. S., Choi, C. S., and Dunn, B. S. (2018). Sulfide solid electrolytes for Lithium battery applications. *Adv. Energy Mater.* 8:1800933. doi: 10.1002/aenm.201800933

Lee, J. W., Lan, P. X., Kim, B., Lim, G., and Cho, D. W. (2008). Fabrication and characteristic analysis of a poly(propylene fumarate) scaffold using micro-stereolithography technology. *J. Biomed. Mater. Res. B Appl. Biomater.* 87, 1–9. doi: 10.1002/jbm.b.31057

Lee, K. W., Wang, S., Fox, B. C., Ritman, E. L., Yaszemski, M. J., and Lu, L. J. B. (2007). Poly(propylene fumarate) bone tissue engineering scaffold fabrication using stereolithography: effects of resin formulations and laser parameters. *Biomacromolecules* 8, 1077–1084. doi: 10.1021/bm060834v

Leijonmarck, S., Cornell, A., Lindbergh, G., and Wågberg, L. (2013). Single-paper flexible Li-ion battery cells through a paper-making process based on nano-fibrillated cellulose. *J. Mater. Chem. A* 1, 4671–4677. doi: 10.1039/c3ta01532g

Lethien, C., Zegaoui, M., Roussel, P., Tilmant, P., Rolland, N., and Rolland, P. A. (2011). Micro-patterning of LiPON and lithium iron phosphate material deposited onto silicon nanopillars array for lithium ion solid state 3D micro-battery. *Microelectron. Eng.* 88, 3172–3177. doi: 10.1016/j.mee.2011.06.022

Lewis, J. A. (2004). Colloidal processing of ceramics. *J. Am. Ceram. Soc.* 83, 2341–2359.

Li, B., Gu, P., Feng, Y., Zhang, G., Huang, K., Xue, H., et al. (2017). Ultrathin Nickel–Cobalt Phosphate 2D nanosheets for electrochemical energy storage under aqueous/solid-state electrolyte. *Adv. Funct. Mater.* 27:1605784. doi: 10.1002/adfm.201605784

Li, C., Liu, Y., Li, B., Zhang, F., Cheng, Z., He, P., et al. (2019). Integrated solid electrolyte with porous cathode by facilely one-step sintering for an all-solid-state Li-O2 battery. *Nanotechnology* 30:364003. doi: 10.1088/1361-6528/ab226f

Li, M., Chen, A.-N., Lin, X., Wu, J.-M., Chen, S., Cheng, L.-J., et al. (2019). Lightweight mullite ceramics with controlled porosity and enhanced properties prepared by SLS using mechanical mixed FAHSs/polyamide12 composites. *Ceram. Int.* 45, 20803–20809. doi: 10.1016/j.ceramint.2019.07.067

Li, S., Zhang, S. Q., Shen, L., Liu, Q., Ma, J. B., Lv, W., et al. (2020). Progress and perspective of ceramic/polymer composite solid electrolytes for Lithium batteries. *Adv. Sci.* 7:1903088.

Li, W., Chen, L., Sun, Y., Wang, C., Wang, Y., and Xia, Y. (2017). All-solid-state secondary lithium battery using solid polymer electrolyte and anthraquinone cathode. *Solid State Ion.* 300, 114–119. doi: 10.1016/j.ssi.2016.12.013

Li, X., Zhang, Z., Yin, K., Yang, L., Tachibana, K., and Hirano, S.-I. (2015). Mesoporous silica/ionic liquid quasi-solid-state electrolytes and their application in lithium metal batteries. *J. Power Sources* 278, 128–132. doi: 10.1016/j.jpowsour.2014.12.053

Li, Y., Ding, F., Xu, Z., Sang, L., Ren, L., Ni, W., et al. (2018). Ambient temperature solid-state Li-battery based on high-salt-concentrated solid polymeric electrolyte. *J. Power Sources* 397, 95–101. doi: 10.1016/j.jpowsour.2018.05.050

Liang, S., Yan, W., Wu, X., Zhang, Y., Zhu, Y., Wang, H., et al. (2018). Gel polymer electrolytes for lithium ion batteries: fabrication, characterization and performance. *Solid State Ion.* 318, 2–18. doi: 10.1016/j.ssi.2017.12.023

Lim, H.-D., Lim, H.-K., Xing, X., Lee, B.-S., Liu, H., Coaty, C., et al. (2018). Solid electrolyte layers by solution deposition. *Adv. Mater. Interfaces* 5:1701328. doi: 10.1002/admi.201701328

Liu, W., Lee, S. W., Lin, D., Shi, F., Wang, S., Sendek, A. D., et al. (2017). Enhancing ionic conductivity in composite polymer electrolytes with well-aligned ceramic nanowires. *Nat. Energy* 2:17035.

Liu, X., Li, X., Li, H., and Wu, H. B. (2018). Recent progress of hybrid solid-state electrolytes for Lithium batteries. *Chemistry* 24, 18293–18306. doi: 10.1002/chem.201803616

Luongo, A., Falster, V., Doest, M. E. B., Ribo, M. M., Eiriksson, E. R., Pedersen, D. B., et al. (2020). Microstructure control in 3D printing with digital light processing. 39, 347–359.

Ma, F., Zhao, E., Zhu, S., Yan, W., Sun, D., Jin, Y., et al. (2016). Preparation and evaluation of high lithium ion conductivity Li1.3Al0.3Ti1.7(PO4)3 solid electrolyte obtained using a new solution method. *Solid State Ion.* 295, 7–12. doi: 10.1016/j.ssi.2016.07.010

Ma, T., and Devin Mackenzie, J. (2019). Fully printed, high energy density flexible zinc-air batteries based on solid polymer electrolytes and a hierarchical catalyst current collector. *Flex. Print. Electron.* 4:015010. doi: 10.1088/2058-8585/ab0b91

Mahajan, A., Frisbie, C. D., and Francis, L. F. (2013). Optimization of aerosol jet printing for high-resolution, high-aspect ratio silver lines. *ACS Appl. Mater. Interfaces* 5, 4856–4864. doi: 10.1021/am400606y

Manapat, J. Z., Chen, Q., Ye, P., and Advincula, R. C. (2017). 3D printing of polymer nanocomposites via stereolithography. *Macromol. Mater. Eng.* 302:1600553. doi: 10.1002/mame.201600553

Manthiram, A., Yu, X., and Wang, S. (2017). Lithium battery chemistries enabled by solid-state electrolytes. *Nat. Rev. Mater.* 2:16103.

Mao, M., He, J., Li, X., Zhang, B., Lei, Q., Liu, Y., et al. (2017). The emerging frontiers and applications of high-resolution 3D printing. *Micromachines* 8:113. doi: 10.3390/mi8040113

Mcowen, D. W., Xu, S., Gong, Y., Wen, Y., Godbey, G. L., Gritton, J. E., et al. (2018). 3D-printing electrolytes for solid-state batteries. *Adv. Mater.* 30:1707132.

Minami, T., Hayashi, A., and Tatsumisago, M. (2006). Recent progress of glass and glass-ceramics as solid electrolytes for lithium secondary batteries. *Solid State Ion.* 177, 2715–2720. doi: 10.1016/j.ssi.2006.07.017

Morimoto, H., Yamashita, H., Tatsumisago, M., and Minami, T. (1999). Mechanochemical synthesis of new amorphous materials of 60Li2S· 40SiS2 with high lithium ion conductivity. *J. Am. Ceram. Soc.* 82, 1352–1354. doi: 10.1111/j.1151-2916.1999.tb01923.x

Naficy, S., Jalili, R., Aboutalebi, S. H., Gorkin Iii, R. A., Konstantinov, K., Innis, P. C., et al. (2014). Graphene oxide dispersions: tuning rheology to enable fabrication. *Mater. Horiz.* 1, 326–331. doi: 10.1039/c3mh00144j

Ngo, T. D., Kashani, A., Imbalzano, G., Nguyen, K. T. Q., and Hui, D. (2018). Additive manufacturing (3D printing): a review of materials, methods, applications and challenges. *Compos. B Eng.* 143, 172–196. doi: 10.1016/j.compositesb.2018.02.012

Nguyen, H., Banerjee, A., Wang, X., Tan, D., Wu, E. A., Doux, J., et al. (2019). Single-step synthesis of highly conductive Na3PS4 solid electrolyte for sodium all solid-state batteries. *J. Power Sources* 435, 126623–126623. doi: 10.1016/j.jpowsour.2019.05.031

Nyman, M., Alam, T. M., Mcintyre, S. K., Bleier, G. C., and Ingersoll, D. (2010). Alternative approach to increasing Li mobility in Li-La-Nb/Ta garnet electrolytes. *Chem. Mater.* 22, 5401–5410. doi: 10.1021/cm101438x

Obata, K., El-Tamer, A., Koch, L., Hinze, U., and Chichkov, B. N. (2013). High-aspect 3D two-photon polymerization structuring with widened objective working range (WOW-2PP). *Light Sci. Appl.* 2:e116. doi: 10.1038/lsa.2013.72

Pang, Y., Cao, Y., Chu, Y., Liu, M., Snyder, K., Mackenzie, D., et al. (2019). Additive manufacturing of batteries. *Adv. Funct. Mater.* 30:1906244.

Park, C.-H., Park, M., Yoo, S.-I., and Joo, S.-K. (2006). A spin-coated solid polymer electrolyte for all-solid-state rechargeable thin-film lithium polymer batteries. *J. Power Sources* 158, 1442–1446. doi: 10.1016/j.jpowsour.2005.10.022

Park, I.-B., Ha, Y.-M., Kim, M.-S., Kim, H.-C., and Lee, S.-H. (2012). Three-dimensional grayscale for improving surface quality in projection microstereolithography. *Int. J. Precis. Eng. Manufact.* 13, 291–298. doi: 10.1007/s12541-012-0036-0

Pesce, A., Hornés, A., Núñez, M., Morata, A., Torrell, M., and Tarancón, A. (2020). 3D printing the next generation of enhanced solid oxide fuel and electrolysis cells. *J. Mater. Chem. A*. doi: 10.1039/d0ta02803g

Pfenninger, R., Struzik, M., Garbayo, I., Stilp, E., and Rupp, J. L. M. (2019). A low ride on processing temperature for fast lithium conduction in garnet solid-state battery films. *Nat. Energy* 4, 475–483. doi: 10.1038/s41560-019-0384-4

Phuc, N. H. H., Totani, M., Morikawa, K., Muto, H., and Matsuda, A. (2016). Preparation of Li3PS4 solid electrolyte using ethyl acetate as synthetic medium. *Solid State Ion.* 288, 240–243. doi: 10.1016/j.ssi.2015.11.032

Pradel, A., Pagnier, T., and Ribes, M. (1985). Effect of rapid quenching on electrical properties of lithium conductive glasses. *Solid State Ion.* 17, 147–154. doi: 10.1016/0167-2738(85)90064-5

Reyes, C., Somogyi, R., Niu, S., Cruz, M. A., Yang, F., Catenacci, M. J., et al. (2018). Three-dimensional printing of a complete lithium ion battery with fused filament fabrication. *ACS Appl. Energy Mater.* 1, 5268–5279.

Ruetschi, P., Meli, F., and Desilvestro, J. (1995). Nickel-metal hydride batteries. The preferred batteries of the future? *J. Power Sources* 57, 85–91. doi: 10.1016/0378-7753(95)02248-1

Ruzmetov, D., Oleshko, V. P., Haney, P. M., Lezec, H. J., Karki, K., Baloch, K. H., et al. (2012). Electrolyte stability determines scaling limits for solid-state 3D Li ion batteries. *Nano Lett.* 12, 505–511. doi: 10.1021/nl204047z

Santoliquido, O., Colombo, P., and Ortona, A. (2019). Additive manufacturing of ceramic components by digital light processing: a comparison between the "bottom-up" and the "top-down" approaches. *J. Eur. Ceram. Soc.* 39, 2140–2148. doi: 10.1016/j.jeurceramsoc.2019.01.044

Schiavo, L. S. A., Mantas, P. Q., Segadães, A. M., and Cruz, R. C. D. (2018). From dry pressing to plastic forming of ceramics: assessing the workability window. *Constr. Build. Mater.* 189, 594–600. doi: 10.1016/j.conbuildmat.2018.09.015

Schnell, J., Günther, T., Knoche, T., Vieider, C., Köhler, L., Just, A., et al. (2018). All-solid-state lithium-ion and lithium metal batteries – paving the way to large-scale production. *J. Power Sources* 382, 160–175. doi: 10.1016/j.jpowsour.2018.02.062

Shan, Y., Li, Y., and Pang, H. (2020). Applications of Tin Sulfide-based materials in Lithium-ion batteries and Sodium-ion batteries. *Adv. Funct. Mater.* 30:2001298. doi: 10.1002/adfm.202001298

Smith, A. J., Burns, J. C., Trussler, S., and Dahn, J. R. (2010). Precision measurements of the coulombic efficiency of Lithium-ion batteries and of electrode materials for Lithium-ion batteries. *J. Electrochem. Soc.* 157: A196.

Strauss, F., Teo, J. H., Schiele, A., Bartsch, T., Hatsukade, T., Hartmann, P., et al. (2020). Gas evolution in Lithium-ion batteries: solid versus liquid electrolyte. *ACS Appl. Mater. Interfaces* 12, 20462–20468.

Sun, C., Fang, N., Wu, D. M., and Zhang, X. (2005). Projection micro-stereolithography using digital micro-mirror dynamic mask. *Sens. Actuators A Phys.* 121, 113–120. doi: 10.1016/j.sna.2004.12.011

Sun, J., Li, Y., Zhang, Q., Hou, C., Shi, Q., and Wang, H. (2019). A highly ionic conductive poly(methyl methacrylate) composite electrolyte with garnet-typed Li6.75La3Zr1.75Nb0.25O12 nanowires. *Chem. Eng. J.* 375:121922. doi: 10.1016/j.cej.2019.121922

Sun, Y., Shi, P., Chen, J., Wu, Q., Liang, X., Rui, X., et al. (2020). Development and challenge of advanced nonaqueous sodium ion batteries. *EnergyChem* 2:100031. doi: 10.1016/j.enchem.2020.100031

Suvacı, E., and Messing, G. L. (2001). Textured alumina ceramics by uniaxial pressing. *Key Eng. Mater.* 206-213, 405–408. doi: 10.4028/www.scientific.net/kem.206-213.405

Takada, K. (2013). Progress and prospective of solid-state lithium batteries. *Acta Mater.* 61, 759–770. doi: 10.1016/j.actamat.2012.10.034

Tallon, C., and Franks, G. V. (2011). Recent trends in shape forming from colloidal processing: a review. 119, 147–160. doi: 10.2109/jcersj2.119.147

Tan, S. J., Zeng, X. X., Ma, Q., Wu, X. W., and Guo, Y. G. (2018). Recent advancements in polymer-based composite electrolytes for rechargeable Lithium batteries. *Electrochem. Energy Rev.* 1, 113–138. doi: 10.1007/s41918-018-0011-2

Tanaka, S., Pin, C. C., and Uematsu, K. (2006). Effect of organic binder segregation on sintered strength of dry-pressed alumina. *J. Am. Ceram. Soc.* 89, 1903–1907. doi: 10.1111/j.1551-2916.2006.01057.x

Tatsumisago, M., and Hayashi, A. (2012). Superionic glasses and glass–ceramics in the Li2S–P2S5 system for all-solid-state lithium secondary batteries. *Solid State Ion.* 225, 342–345. doi: 10.1016/j.ssi.2012.03.013

Teragawa, S., Aso, K., Tadanaga, K., Hayashi, A., and Tatsumisago, M. (2014). Preparation of Li2S–P2S5 solid electrolyte from N-methylformamide solution and application for all-solid-state lithium battery. *J. Power Sources* 248, 939–942. doi: 10.1016/j.jpowsour.2013.09.117

Trevey, J., Jang, J. S., Jung, Y. S., Stoldt, C. R., and Lee, S. H. (2009). Glass–ceramic Li2S–P2S5 electrolytes prepared by a single step ball billing process and their application for all-solid-state lithium–ion batteries. *Electrochem. Commun.* 11, 1830–1833. doi: 10.1016/j.elecom.2009.07.028

Truby, R. L., and Lewis, J. A. (2016). Printing soft matter in three dimensions. *Nature* 540, 371–378. doi: 10.1038/nature21003

Tumbleston, J. R., Shirvanyants, D., Ermoshkin, N., Janusziewicz, R., Johnson, A. R., Kelly, D., et al. (2015). Continuous liquid interface production of 3D objects. *Science* 347, 1349–1352. doi: 10.1126/science.aaa2397

Varshneya, A. K., and Mauro, J. C. (2019). *Fundamentals of Inorganic Glasses*. Amsterdam: Elsevier.

Venkatasubramanian, N., Wade, B., Desai, P., Abhiraman, A., and Gelbaum, L. (1991). Synthesis and characterization of spinnable sol-gel derived polyborates. *J. Non Cryst. Solids* 130, 144–156. doi: 10.1016/0022-3093(91)90450-k

Wan, J., Xie, J., Kong, X., Liu, Z., Liu, K., Shi, F., et al. (2019). Ultrathin, flexible, solid polymer composite electrolyte enabled with aligned nanoporous host for Lithium batteries. *Nat. Nanotechnol.* 14, 705–711. doi: 10.1038/s41565-019-0465-3

Wang, L., Ye, Y., Chen, N., Huang, Y., Li, L., Wu, F., et al. (2018). Development and challenges of functional electrolytes for high-performance Lithium-Sulfur batteries. *Adv. Funct. Mater.* 28:1800919. doi: 10.1002/adfm.201800919

Wang, X. J., Zhang, H. P., Kang, J. J., Wu, Y. P., and Fang, S. B. (2005). Novel composite polymer electrolytes based on poly(ether-urethane) network polymer and fumed silicas. *J. Solid State Electrochem.* 11, 21–26. doi: 10.1007/s10008-005-0029-3

Warner, J. T. (2015). *The Handbook of Lithium-Ion Battery Pack Design: Chemistry, Components, Types and Terminology*. Amsterdam: Elsevier.

Wei, T. S., Ahn, B. Y., Grotto, J., and Lewis, J. A. (2018). 3D printing of customized Li-ion batteries with thick electrodes. *Adv. Mater.* 30:1703027. doi: 10.1002/adma.201703027

Wootthikanokkhan, J., Phiriyawirut, M., and Pongchumpon, O. J. (2015). Effects of electrospinning parameters and nanofiller content on morphology and gel electrolyte properties of composite nanofibers based on La2O3-Filled PVDF-HFP. *Int. J. Polym. Mater. Polym. Biomater.* 64, 416–426. doi: 10.1080/00914037.2014.958830

Xie, J., Imanishi, N., Zhang, T., Hirano, A., Takeda, Y., and Yamamoto, O. (2009). Li-ion transport in all-solid-state lithium batteries with LiCoO2 using NASICON-type glass ceramic electrolytes. *J. Power Sources* 189, 365–370. doi: 10.1016/j.jpowsour.2008.08.015

Xing, B., Yao, Y., Meng, X., Zhao, W., Shen, M., Gao, S., et al. (2020). Self-supported yttria-stabilized zirconia ripple-shaped electrolyte for solid oxide fuel cells application by digital light processing three-dimension printing. *Scr. Mater.* 181, 62–65. doi: 10.1016/j.scriptamat.2020.02.004

Yang, Y., Chen, Z., Song, X., Zhu, B., Hsiai, T., Wu, P.-I., et al. (2016). Three dimensional printing of high dielectric capacitor using projection based stereolithography method. *Nano Energy* 22, 414–421. doi: 10.1016/j.nanoen.2016.02.045

Yang, Y., Yuan, W., Zhang, X., Yuan, Y., Wang, C., Ye, Y., et al. (2020). Overview on the applications of three-dimensional printing for rechargeable lithium-ion batteries. *Appl. Energy* 257:14002.

Yin, Y. C., Wang, Q., Yang, J. T., Li, F., Zhang, G., Jiang, C. H., et al. (2020). Metal chloride perovskite thin film based interfacial layer for shielding Lithium metal from liquid electrolyte. *Nat. Commun.* 11:1761.

Yoshio, M., Brodd, R. J., and Kozawa, A. (2009). *Lithium-Ion Batteries*. New York, NY: Springer.

Yuan, M., and Liu, K. (2020). Rational design on separators and liquid electrolytes for safer lithium-ion batteries. *J. Energy Chem.* 43, 58–70. doi: 10.1016/j.jechem.2019.08.008

Yue, L., Ma, J., Zhang, J., Zhao, J., Dong, S., Liu, Z., et al. (2016). All solid-state polymer electrolytes for high-performance lithium ion batteries. *Energy Storage Mater.* 5, 139–164.

Zekoll, S., Marriner-Edwards, C., Hekselman, A. K. O., Kasemchainan, J., Kuss, C., Armstrong, D. E. J., et al. (2018). Hybrid electrolytes with 3D bicontinuous ordered ceramic and polymer microchannels for all-solid-state batteries. *Energy Environ. Sci.* 11, 185–201. doi: 10.1039/c7ee02723k

Zhang, H., Li, C., Piszcz, M., Coya, E., Rojo, T., Rodriguez-Martinez, L. M., et al. (2017). Single lithium-ion conducting solid polymer electrolytes: advances and perspectives. *Chem. Soc. Rev.* 46, 797–815.

Zhang, Q., Cao, D., Ma, Y., Natan, A., Aurora, P., and Zhu, H. (2019). Sulfide-based solid-state electrolytes: synthesis, stability, and potential for all-solid-state batteries. *Adv. Mater.* 31:e1901131.

Zhang, S. S. (2007). A review on the separators of liquid electrolyte Li-ion batteries. *J. Power Sources* 164, 351–364. doi: 10.1016/j.jpowsour.2006.10.065

Zhang, X., Liu, T., Zhang, S., Huang, X., Xu, B., Lin, Y., et al. (2017). Synergistic Coupling between Li6.75La3Zr1.75Ta0.25O12 and poly(vinylidene fluoride) induces high ionic conductivity, mechanical strength, and thermal stability of solid composite electrolytes. *J. Am. Chem. Soc.* 139, 13779–13785. doi: 10.1021/jacs.7b06364

Zhou, Q., Zhang, J., and Cui, G. (2018). Rigid–flexible coupling polymer electrolytes toward high-energy lithium batteries. *Macromol. Mater. Eng.* 303:1800337. doi: 10.1002/mame.201800337

Conflict of Interest: The authors declare that the research was conducted in the absence of any commercial or financial relationships that could be construed as a potential conflict of interest.